**Combustion Instability and Blowout Characteristics of Fuel Flexible Combustors**


**Final Report**


**Reporting Period Start Date:  February 1, 2004**

**Reporting Period End Date:  December 31, 2006**


**Principal Investigators: Tim Lieuwen and Ben Zinn**


**Date Report was issued  January 31, 2007**


**DOE Award Number  O3-O1-SR111**


**School of Aerospace Engineering**

**Georgia Institute of Technology**

**Atlanta, GA 30332-0150**

**DISCLAIMER:**

# 1.    ABSTRACT

Under this program, Georgia Institute of Technology investigated the blowout characteristics of fuel-flexible combustors.  Particular attention was given to coal-derived and high hydrogen gaseous fuels which are of interest to the DOE.  The program consists of three main focuses.

Under the first research focus, we performed extensive chemical kinetic analyses of such quantities as flame speeds and stretch sensitivities of syngas fuels in order to develop the mixture characteristics information needed to correlate test data.  In addition, we developed and distributed a software utility that utilizes these calculations, determines other basic mixture properties, and has such features as outputting all fuel mixture combinations with a given flame speed, adiabatic flame temperature, or heating value within some given tolerance.

Under the second research focus, we made extensive measurements of the combustor's blowout characteristics as a function of fuel composition.  We designed and fabricated a gas-mixing facility to blend syngas-type fuels of arbitrary compositions of $H_2$, CO, $CO_2$, $N_2$, and $CH_4$.  We then measured the equivalence ratios at lean blow off for a large number of $H_2$/CO/$CH_4$ mixtures at different inlet temperatures and combustion pressures.  Consistent with prior studies, these results indicate that the percentage of $H_2$ in the fuel dominates the mixture blowout characteristics.  It is shown that standard well stirred reactor based correlations, based upon a Damköhler number with a diffusivity ratio correction, can capture the effects of fuel composition variability on blowoff limits.

Under the third research focus, we performed more detailed diagnostics of near blowoff flames in order to characterize the blowoff phenomenology better and to provide further insight into how fuel composition (particularly $H_2$ levels in the fuel) alters this phenomenology.  This was accomplished through high speed visualizations of the flame and velocity field measurements.  Near blowoff, a variety of highly dynamic flow features are observed, which vary substantially with the $H_2$ levels in the fuel.  These features involve complex interactions between the vortex breakdown bubble, outer recirculation zone of the rapid expansion, and flame extinction/reignition phenomenon.

## 2. TABLE OF CONTENTS

# 3.    LIST OF FIGURES

# 4. EXECUTIVE SUMMARY

Under this program, Georgia Institute of Technology investigated the blowout characteristics of fuel-flexible combustors. Particular attention was given to coal-derived and high hydrogen gaseous fuels which are of interest to the DOE. This work is motivated by the fact that the inherent variability in composition and heating value of coal derived and other alternative fuels provides one of the largest barriers towards their usage. This fuel composition variability is of concern because low emissions combustion systems are generally optimized to operate with fuels that meet tight specifications. The successful completion of this project has benefited the nation by removing barriers toward the usage of coal derived gaseous fuels through improved understanding of their combustion characteristics. Ultimately, these benefits will increase the air quality and energy security of the USA, by allowing power plants to operate efficiently and with minimal pollution, using a variety of domestic fuel sources.

The program consists of three main focuses. Under the first research focus, we performed extensive chemical kinetic analyses of such quantities as flame speeds and stretch sensitivities of syngas fuels in order to develop the mixture characteristic information needed to correlate test data. In addition, we developed and distributed a software utility that utilizes these calculations, determines other basic mixture properties, and has such features as outputting all fuel mixture combinations with a given flame speed, adiabatic flame temperature, or heating value within some given tolerance.

Under the second research focus, we made extensive measurements of the combustor's blowout characteristics as a function of fuel composition. We designed and fabricated a gas-mixing facility to blend syngas-type fuels of arbitrary compositions of $H_2$, CO, $CO_2$, $N_2$, and $CH_4$. We then measured the equivalence ratios at lean blow off for a large number of $H_2$/CO/$CH_4$ mixtures at different inlet temperatures and combustion pressures. Consistent with prior studies, these results indicate that the percentage of $H_2$ in the fuel dominates the mixture blowout characteristics. It is shown that standard well stirred reactor based correlations, based upon a Damköhler number with a diffusivity ratio correction, can capture the effects of fuel composition variability on blowoff limits. In addition, visual observations indicate that the blowoff phenomenology qualitatively changes with hydrogen levels in the fuel, being very different for mixtures with $H_2$ levels above and below about 50%.

Under the third research focus, we performed more detailed diagnostics of near blowoff flames in order to characterize the blowoff phenomenology better and to provide further insight into how fuel composition (particularly $H_2$ levels in the fuel) alters this phenomenology. This was accomplished through high speed visualizations of the flame and velocity field measurements. Near blowoff, a variety of highly dynamic flow features are observed, which vary substantially with the $H_2$ levels in the fuel. These features involve complex interactions between the vortex breakdown bubble, outer recirculation zone of the rapid expansion, and flame extinction/reignition phenomenon.

# 5. PROJECT DESCRIPTION

Modern power turbines have the highest operating efficiencies and turn out fewer pollutants than other major combustion energy converting devices[1]. In addition, the low capital costs required to bring a new system online have made them attractive to investors. As a result, gas turbines have become the dominant technology for new power generating capacity in the U.S. and worldwide. These systems have met their aggressive emission targets by operating in a lean, premixed mode of combustion. This mode of burning has significant advantages over its nonpremixed counterpart in achieving low pollutant emissions, particularly in regards to $NO_x$ and soot.[2]

Current low emissions technology primarily focuses on burning natural gas, a fuel that is mainly composed of methane. It seems clear, however, that natural gas cannot be relied upon as the exclusive source for fueling the clean power plants of the future. Rapidly increasing demand due to new installations has caused substantial price volatility and concerns about future supplies. In addition, interest in utilizing the United State's other energy resources, as well as concern about energy security have motivated interest in utilizing coal-derived syngas or fuels from other sources, such as biomass, landfill gas, process gas and others. The development of clean coal technologies is particularly compelling given the fact that coal is the United State's most abundant fuel source. Technologies such as integrated gasification combined cycle (IGCC) plants enable the combustion of coal and other solid or liquid fuels, while still maintaining aggressive emissions targets and high efficiency.

The inherent variability in composition and heating value of these fuels provides one of the largest barriers towards their usage, however. Syngas fuels are typically composed primarily of $H_2$, CO, and $N_2$, and may also contain smaller amounts of methane ($CH_4$), $O_2$, $CO_2$, and other higher order hydrocarbons.[3] The primary constituents of landfill or sewage gas are typically $CH_4$ and $CO_2$.[4] Depending upon the source and particular processing technique, these fuels can have significant ranges in relative composition of these constituents.

This variability is a significant problem because state-of-the-art low emission combustion systems are typically optimized to operate with fuels that meet tight fuels specifications. Specifications for gas fuels cover parameters such as heating value, hydrogen content, and solid

contaminant levels. Expensive test programs and hardware modifications are generally required if there are significant changes to gas fuel properties.

The objective of this program is to improve the state of the art in understanding and modeling lean blowout in low emissions, fuel-flexible gas turbines. Successful completion of this project benefits the gas turbine and energy industry in several ways. It will remove barriers toward the usage of coal derived gaseous fuels through improved understanding of their combustion characteristics. It will also improve the development of modeling tools needed by OEM's to design fuel-flexible combustion systems. Ultimately, these benefits will increase the air quality and energy security of the USA, by allowing power plants to operate efficiently and with minimal pollution, using a variety of domestic fuel sources.

# 6. KEY VARIAB LES AND MECHANISMS FOR LEAN BLOWOFF

## *BACKGROUND*

Flame stabilization involves competition between the rates of the chemical reactions and the rates of turbulent diffusion of species and energy.  While a significant amount of fundamental understanding of flame propagation and stability characteristics of lean, premixed systems has been gained in conventionally fueled, natural gas-air systems[5], little is known about these issues for alternate gaseous fuels, such as syngas or low BTU fuel mixtures.  Furthermore, the majority of the fundamental investigations of the combustion characteristics of these synthetic gases are for nonpremixed flame configurations [6,7,8,9,10].

Consider syngas fuels which are composed primarily of $H_2$, CO and $N_2$.  Both $H_2$ and CO act as fuels when oxidized. Individually, they produce higher adiabatic flame temperatures (at stoichiometric conditions in air) than $CH_4$, 2383 and 2385 K, as compared to 2220 K.  $H_2$ and CO also have lower flammability limits ($\phi$=0.14 and 0.34, respectively) than $CH_4$ ($\phi$=0.46), and higher maximum adiabatic laminar flame speeds (320 and 55 cm/s versus 40 cm/s for methane)[ 11 ].   This would suggest that these fuels could have better flame holding characteristics than natural gas.   The picture for the pure fuels becomes slightly more complicated at lean mixtures, however, because the flame speed of CO drops below that of $CH_4$. This comparison of pure fuels does not, however, paint a complete picture.   The turbulent propagation and stability properties of premixed $H_2$/CO mixtures are not well documented, and performance characteristics of these mixtures cannot be simply inferred from knowledge of the global performance of the constituents.   To begin, CO and $H_2$ have *significantly* different transport properties and flame speeds.   Next, CO chemistry, which releases slightly more heat than the same amount of $H_2$ by mass, is highly coupled to $H_2$ oxidation through the reaction $CO+OH \rightarrow CO_2+H$, which dominates CO ignition (at least) at atmospheric pressure.

The coupling is also important in that, together, CO and $H_2$ oxidation can cover a wide range of time scales that may bridge the relevant fluid dynamic, turbulent time scales.  As shown below, chemical time scales of $CO/H_2$ mixtures are quite different, and given the large spectrum of turbulent time scales in practical combustors, the combustion processes can cover several orders of magnitude of Damköhler number.  For example, interactions between turbulent mixing

processes and, say, $H_2$ oxidation may occur in the "flamelet" regime, those associated with CO oxidation in a "torn flamelets" regime, and OH recombination (whose chemistry plays a key role in CO oxidation) in the distributed reaction regimes. Furthermore, the oxidation and, hence, rates of heat release of CO and $H_2$ display different or opposite sensitivities to mean pressure or flame strain/ stretch imposed by the turbulent flow field.

In addition, syngas fueled plants sometimes co-fire with a certain fraction of natural gas, so the additional interactions associated with $H_2/CH_4$ flame and $CO/CH_4$ flame also need to be considered. Several recent studies have focused on $H_2/CH_4$ flames [16,17] and shown that small additions of $H_2$ substantially enhances the mixture's resistance to extinction or blowoff. For example, fundamental studies in opposed flow burner geometries show that the extinction strain rate of methane flames is doubled with the addition of 10% $H_2$[12,13]. The acceleration of the $CH_4$ reaction rate by the radical pool created by the early breakdown of $H_2$ has been suggested as a key mechanism for this behavior.

$CO/CH_4$ flames also have interesting dynamics because of their coupled chemistry. The CO burning rate is highly dependent on the reaction $CO+OH \rightarrow CO_2+H$. Addition of $CH_4$ increases the radicals for this reaction. In addition, CO is also believed to be a significant intermediate during the low temperature reaction path of $CH_4$ [14].

The above discussion clearly indicates the need for more extensive systematic studies of the blowout characteristics of premixed flames using the fuels that will be encountered in fuel-flexible combustors. Several studies have been initiated relatively recently to investigate the characteristics of premixed, hydrogen-enriched methane fuels [15,16,17]. Additional studies are needed, however, to broaden the scope of fuels of interest.

Having briefly considered the kinetic characteristics of these fuels, we turn attention next to issues associated with blowoff. Developing physics-based correlations of blowout behavior is complicated by lack of understanding of the flame characteristics at the stabilization point. Currently, there is disagreement on whether premixed flames in high turbulent intensity gas turbine environments have flamelet, "thickened" flamelet, or well stirred reactor (WSR) – like properties.

Methods for developing blowout correlations in the latter case (i.e., using WSR scaling ideas) have been studied extensively. Several different theories or physical considerations have been used in past blowout correlation studies, such as those of Zukoski and Marble [18],

Spalding [19], or Longwell[20]. As noted by Glassman [11], however, they lead to essentially the same form of correlation. These correlations generally involve relating the blowoff limits to a ratio of a chemical kinetic time and residence time, $\tau_{chem}/\tau_{res}$. In well stirred reactor theory, this ratio is often referred to as a combustor loading parameter. It is possible that the recirculation regions that stabilize many high intensity flames, which may have flamelet properties at most other points along the flame, have distributed reactor-like properties; hence, the success in WSR models in correlating blowout behavior.

When applied to blowoff limits of premixed flames, this chemical time is typically estimated as:

$$\tau_{chem} = \alpha / S_L^2 \quad (1)$$

where $S_L$ and $\alpha$ denote the laminar flame speed and thermal diffusivity, respectively[21,22]. Alternative methods of estimating a global chemical time are also possible, but generally lead to results qualitatively similar to Eq. (1). For example, **Figure 1** compares the blowoff residence time of a well stirred reactor model to the chemical time from Eq. (1) for several $H_2/CO/CH_4$ mixtures (the color of each point uniquely represents its composition, as will be explained below). The two time scales are closely related, except for cases with very high CO mixtures (not shown).
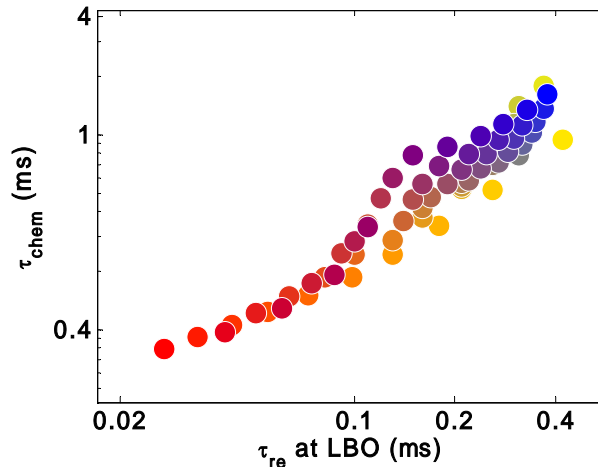


**Figure 1: Relationship between chemical time calculated using Eq. (1) and blowout residence time for $\phi$=0.6 $H_2/CO/CH_4$ mixtures. Results obtained using AURORA and TRAN in CHEMKIN with GRI 3.0 mechanism**

Returning to WSR based methods for scaling blowoff limits, the residence time is generally scaled as $d/U_{ref}$, where $d$ and $U_{ref}$ denote a characteristic length scale (e.g., a recirculation zone length) and velocity scale, respectively. If this reactor based theory is correct, then blowoff limits should scale with the loading parameter:

$$L_1 = \frac{\tau_{chem}}{\tau_{res}} = \frac{\alpha U_{ref}}{S_L^2 d} \qquad (2)$$

This "loading parameter" correlation is equivalent to Peclet number correlations which are also used[23]. Defining Peclet numbers based upon flame and flow velocity: $Pe_u = U_{ref}d/\alpha$ and $Pe_{SL} = S_L d/\alpha$, note that:

$$L_1 = \frac{Pe_u}{Pe_{SL}^2} \qquad (3)$$

These purely combustion considerations are incomplete without consideration of the corresponding fluid mechanics, however. For example, note that $U_{ref}$ need not directly scale with approach flow velocity, $U_u$, due to the acceleration of the burned gas[21]. Since the burned gas velocity scale is given by $U_b = (T_b/T_u)U_u$, then $U_{ref} = f(U_u, T_b/T_u)$. Similar considerations apply for the recirculation zone scale, $d$. For this reason, prior workers have often had to measure the recirculation zone length in order to use Eq. (2) (e.g., see Ref. 18).

The work of Hoffman *et al.*[24] is of special interest, as it found good success with the Peclet number correlation of Eq. (3) to capture the dependence of blowoff limits in swirling, premixed flames upon combustor diameter, flow velocity, and swirl number. They used the azimuthal velocity component, $U_\theta$, as the reference velocity, $U_{ref} = U_\theta$, and combustor diameter, $D$, as the characteristic length, $D = d$.

Significantly less attention has been given to correlating premixed flame blowout limits assuming flamelet-like combustion properties, where the stabilization mechanism is related to front propagation, rather than reactor extinction. In this case, a flame would blow off when the turbulent flame speed is everywhere less than the flow velocity, $S_T < U_{ref}$, where $S_T$ denotes the turbulent flame speed. If this propagation mechanism is controlling, then blowoff limits should scale with the parameter:

$$L_2 = \frac{S_T}{U_{ref}} \qquad (4)$$

Evaluating the turbulent flame speed introduces additional complications for mixtures with widely varying compositions. Correlations of the turbulent flame speed of the form: $S_T=S_L \cdot f(u',$geometry$)$, where $u'$ denotes turbulent intensity, have been used successfully in many prior studies across limited fuel ranges. However, recent studies across broader ranges of fuels clearly indicate the limitations of the above correlation; other fuel properties are also very important.

For                                                                example,

**Figure 2** is reproduced from Kido *et al.*[25 ]and plots the dependence of the turbulent flame speed for a variety of $H_2$, $CH_4$, and $C_3H_8$ mixtures. These mixtures were carefully chosen to have identical laminar flame speeds, as indicated by the $S_T$ curves converging at $u'=0$. Interestingly, however, the curves widely diverge as $u'$ increases from zero. In particular, note the substantially higher turbulent flame speed of the H07-15N mixture, which is a hydrogen blend, relative to the methane fuels (MO7-15N, M09-15N, MO98-15N).

**Figure 2: Dependence of turbulent flame speed upon turbulence intensity for several fuel blends with the same laminar flame speed (reproduced from Kido *et al.* [25]).**
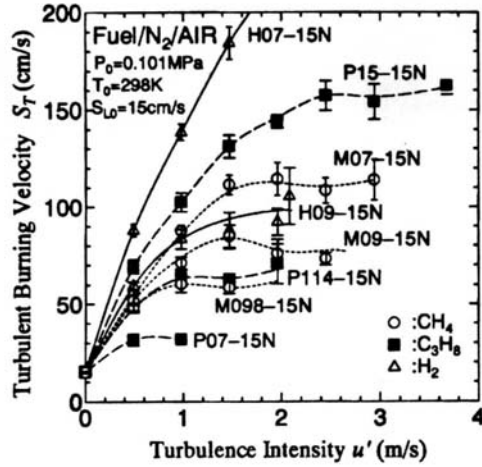
| Mixture | Fuel | O$_2$ | N$_2$ | $\phi$ | $S_{L0}$ (cm/s) |
|---|---|---|---|---|---|
| | | Molar Fraction | | |
| H07-15N | H$_2$ | 0.71 | 7.14 | 0.7 | 15.26 |
| H09-15N | H$_2$ | 0.56 | 6.94 | 0.9 | 15.88 |
| M07-15N | CH$_4$ | 2.86 | 11.17 | 0.7 | 15.10 |
| M09-15N | CH$_4$ | 2.22 | 10.82 | 0.9 | 14.91 |
| M098-15N | CH$_4$ | 2.04 | 10.51 | 0.98 | 14.84 |
| P07-15N | C$_3$H$_8$ | 7.14 | 29.05 | 0.7 | 14.94 |
| P114-15N | C$_3$H$_8$ | 4.39 | 23.82 | 1.14 | 15.34 |
| P15-15N | C$_3$H$_8$ | 3.33 | 13.70 | 1.5 | 14.99 |

This substantial increase in the turbulent flame speed of the hydrogen mixture my be due to thermal-diffusive instabilities of lean hydrogen mixtures; that is, these mixtures are unstable even in the absence of turbulence, resulting in the spontaneous wrinkling of the premixed flame[26]. This conclusion is supported by related studies that compare the turbulent flame speeds of thermo-diffusively stable/unstable mixtures with the same laminar flame speeds (e.g., by comparing rich and lean methane mixtures) that also show that the unstable mixtures have higher flame speeds [27].

These instabilities can be related to the stretch sensitivity of the flame speed. Recall that the flame speed of a stretched flame is given as [27]:

$$\frac{S_L}{S_{L,0}} = 1 - MaKa \qquad (5)$$

where $S_{L,0}$, $Ma$, and $Ka$, denote the unstretched laminar flame speed, $Ma = L/\delta$ (Markstein number), and $Ka = \tau_{chem}/\tau_k$ (Karlovitz number), respectively. $L, \delta$ and $\tau_k$ denote Markstein length, flame thickness, and Kolmogorov time scale. Thermo-diffusively unstable flames have negative Markstein numbers, which cause bulges in the flame to grow.

Some insight into the key parameters influencing *Ma* can be obtained from asymptotic results with single step kinetics[26]:

$$Ma = \frac{1}{\gamma}\ln\frac{1}{1-\gamma} + \frac{Ze(Le-1)}{2}(\frac{1-\gamma}{\gamma})\int_0^{\gamma/1-\gamma}\frac{\ln(1+x)}{x}dx \qquad (6)$$

where $Ze = \frac{E}{RT_b^2}(T_b - T_u)$ and $\gamma = (T_b - T_u)/T_b$ denote the Zeldovich number and gas expansion parameter, respectively. This equation shows that *Ma* depends upon the gas expansion ratio, dimensionless activation energy and Lewis number. While the general relationship between these quantities is complex, for large *Ze* values. *Ma* has positive and negative values when *Le* > 1 and *Le* < 1, respectively.

## *EXPERIMENTAL SETUP*

**High Pressure Gas Turbine Simulator**
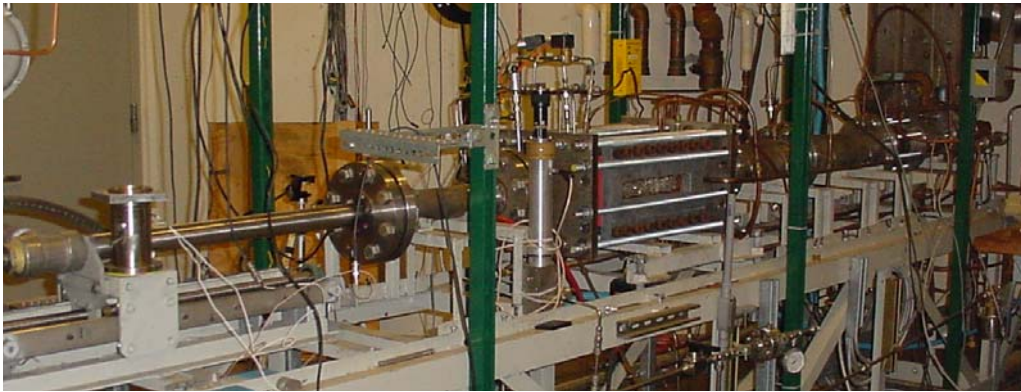


**Figure 3: Photograph of lean, premixed combustor facility**

Measurements were obtained in a lean, premixed gas turbine combustor simulator, shown in **Figure 3,** which has also been previously described in Ref. [28]. The facility consists of inlet/premixer, combustor, and exhaust sections. High-pressure natural gas and air are supplied

from building facilities. The air can be preheated up to 700 K. The hydrogen and carbon monoxide are supplied from bottles. The air and fuel flow rates are measured with a critical orifice and mass flow controllers (MFC's), respectively. Both the orifice and MFC's were calibrated using the specific gas with which they were to meter. This is necessary for $H_2$ in particular, as manufacturer supplied corrections that relate the flow of some other gas to the $H_2$ flow rate were found to be very inaccurate. The resultant uncertainty in the flow rate measurements is 2% of full scale. While only three fuels ($H_2$, CO, and $CH_4$) were used in this study, the system has capabilities to mix a total of six gases, in order to simulate a wide range of fuel blends of arbitrary compositions. In order to ensure that acoustic oscillations did not affect the fuel/air mixing processes, the fuel and air are mixed upstream of a second choke point. Thus, the equivalence ratio of the reactive mixture entering the flame is constant. The temperature of the reactants was measured with a thermocouple located just upstream of the swirler.

The fuel-air mixture entered the circular 4.75 cm diameter, 60 cm long inlet section and passed through a premixer with a swirler prior to entering the combustor, see **Figure 4**, (note that the word "premixer" is somewhat of a misnomer in this case as the fuel and air are already fully premixed). The premixer outer body slightly constricts along the axial flow direction. However, the overall flow area remains constant at 10.8 cm$^2$, as the center body diameter also decreases in the axial flow direction. This premixer is fully modular as the centerbody and swirler can be easily removed and replaced; however, these tests were performed with a single 12 vane, 35$^o$ swirler. Moreover, a thermocouple is imbedded in the centerbody for flashback detection.
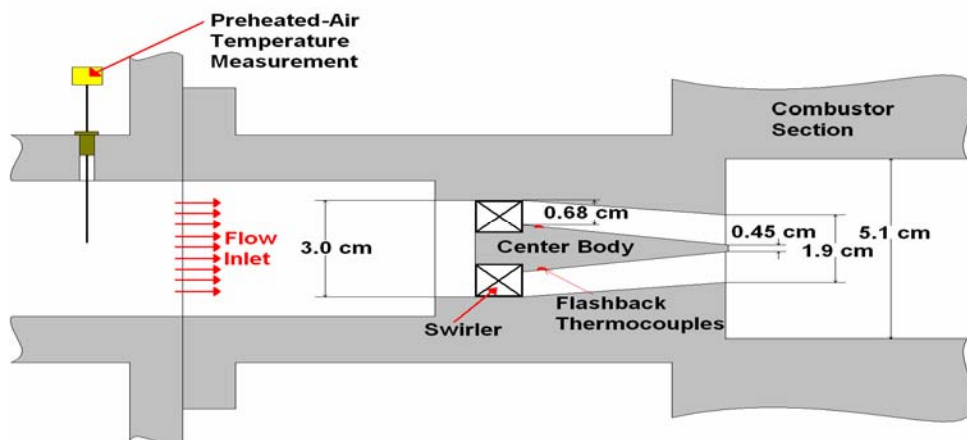


**Figure 4: Cross section of premixer assembly**

The premixer terminates into the 5x5 cm square combustor. The square part of the combustor is 51 cm long and optically accessible. It then transitions into a circular 7.6 cm diameter, 195 cm long exhaust section. The exhaust sections are water cooled[1]. The flow leaves the setup through an exhaust nozzle with an adjustable bypass valve. This adjustable bypass valve is controlled by LabVIEW in order to maintain the combustor pressure at some prescribed value.

**Gas Mixing Facility**

We designed and fabricated a Gas Mixing Facility. The development involved four main considerations and components: (i) bottle storage facility, (ii) bottle valving and controls, (iii) flow control and mixing, and (iv) safety.

*Bottle Storage Facility*

The bottle storage facility is an important aspect of the overall facility because of the safety and functional issues arising from the use of hydrogen and carbon monoxide. The special consideration involves the storage/use of the bottles not only during testing, but during non-operational periods. The final solution has been chosen because of concerns of safety and fire and building codes. The facility is comprised of two indoor storage cabinets, of which one will store three bottles of hydrogen and the other will store three bottles of carbon monoxide. Nitrogen and carbon dioxide bottles are stored in bottle racks in the test room. The gas cabinets are continuously vented by a negative pressure system. These cabinets are explosion proof with double doors and access windows on each door for safe valve/regulator adjustments. These cabinets are equipped with fire sprinklers.

---

[1] Note that the combustor top and bottom walls are water cooled and side walls are air cooled[28]. The combustor was only water cooled for these measurements, since we determined that some leakage of the sideflow cooling air impacted blowout limits.

**Figure 5: Gas Storage Cabinets for Hydrogen and Carbon Monoxide Gas**



**Figure 6: Bottle Storage for Carbon Dioxide and Nitrogen**

*Bottle Valving and Controls*

The bottle valving and controls are crucial to safely and efficiently transporting the syngas components to the combustor. Since the bottles are stored near the inlet of the combustor, the gases are piped overhead and brought down to the combustor. For the hydrogen and carbon monoxide bottles, the valving and controls are inside the cabinets so that if a leak occurred, the gas would be vented out. For these two gases, the three bottles of each gas were manifolded together. Each bottle has a flow limiter and check valve to prevent other bottles from leaking or a catastrophic venting of the gas. After the flow limiters and check valves, the gases are piped to a dual stage regulator for each gas so that the gases can be regulated between 0 and 500 psi. After the regulators, there is a pressure relief valve that releases to the exhaust vents in case a regulator failure occurs. Once the gases pass through the pressure relief valve, a block and bleed

valve combination is used. Both of these valves are electric, hazardous duty valves that can be controlled from the control room facility and automatically controlled by the safety system in case a leak occurs. The valving and controls are similar for the carbon dioxide and nitrogen, where the only difference is that the pressure relief valves and bleed valves are not included. Note that the block valves for the carbon dioxide and nitrogen are controllable by the user in the safe confines of the control room. The safety system does not block and bleed the nitrogen and carbon monoxide, because these gases will purge the fuel feed lines to the combustor. From the block and/or bleed valves, the gases are individually pipe overhead to the combustor.



**Figure 7: Bottle Valving and Controls for Hydrogen and Carbon Monoxide**



**Figure 8: Bottle Valving and Controls for Carbon Dioxide (Left) and Nitrogen (Right)**

*Flow Control and Mixing*

Once the gases are piped overhead, flow controls are necessary. The individual gases are plumbed to mass flow controllers that are remotely controlled by a LabView VI which linearly proportions an input voltage depending on the flow required. The input voltage is between 0 and 5VDC and is compared to a 5VDC reference signal to acquire the proper mass flow rate. These mass flow controllers are from AALBORG which are calibrated with nitrogen gas; thus a $c_p$ correction must be made in the VI if another gas is used. After the mass flow controllers, the gases are combined into one line. This line is piped to a back pressure regulator which is necessary for the proper operation of the mass flow controllers. The back pressure regulator is remotely controlled by low pressure nitrogen gas, so that adjustments can be made without going into the test room. The mixed gas line is then connected with the natural gas line, which is then fed into the combustor.
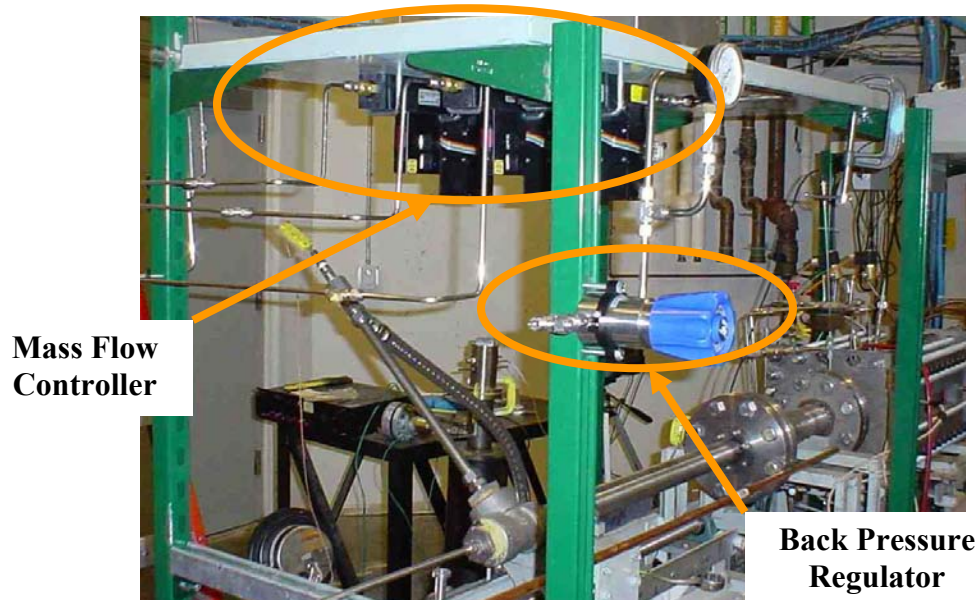


**Figure 9: Mass Flow Controllers and Back Pressure Regulator**
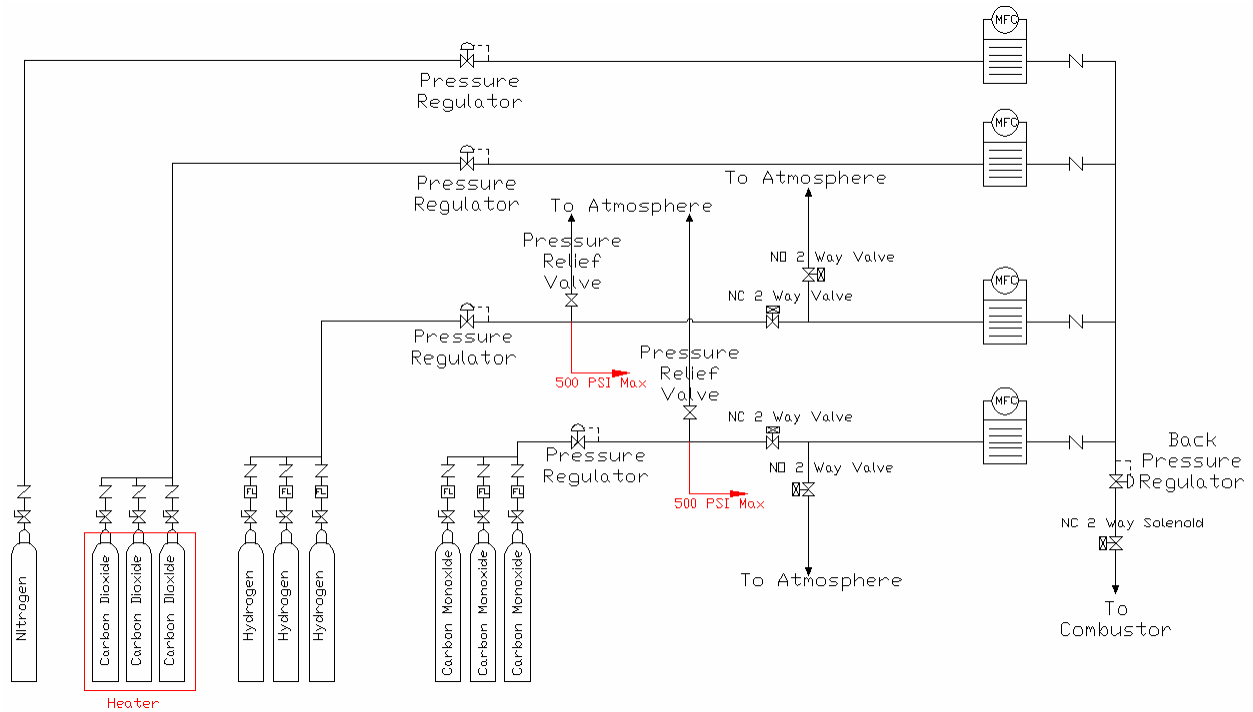
**Figure 10: Full Piping Layout for Syngas System**

*Safety*

Safety was a major focus during this project. An extensive plan was developed to monitor the cabinets and rooms affected by the hydrogen and carbon monoxide gases. This plan includes the active control integration of seven sensors: three hydrogen sensors, three carbon monoxide sensors, and one vacuum sensor. Hydrogen and carbon monoxide sensors are in the cabinets, the combustor room, and the associated control room. Also, there is a vacuum switch on the ventilation stack of the gas cabinets to ensure the system is working.
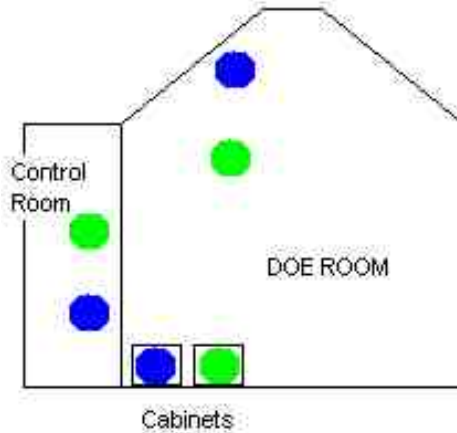
**Figure 11:  Laboratory Sensor Layout (Green--Hydrogen Sensor & Blue--Carbon Monoxide Sensor)**

These sensors are integrated into an active control system.  The system uses relays, sirens, strobe lights, and LED's to alert and safeguard the researchers operating in the control room and those near the high-pressure laboratory from gas leaks.  If any of the sensors are tripped by a gas leak, a color coded LED and strobe light are illuminated alerting the location of the hazardous area.  A tone-coded siren is alarmed, as well as a clear strobe and siren outside the high pressure room.  As an added safety feature, the hydrogen and carbon monoxide gas lines block and bleed if a leak occurs.  This action is delayed by 10 seconds to ensure that the alarm is not a false alert.  Note that the delay does not occur for the low level alarm for the CO sensor in the gas cabinet because it has a dual stage alarm to eliminate false alerts.  Moreover, the user can reset the siren for 30 seconds with a momentary push button on the control panel, as well as override the block/bleed action if the gas detection is known to be false.  The override can only occur if the user holds down a momentary push button on the control panel.  Moreover, the vacuum switch for the ventilation will alert the users that the ventilation fan is not working with a siren and strobe light.  In addition to the alarms, the lack of ventilation in the cabinets blocks and bleeds the hydrogen and carbon monoxide from being distributed.  Importantly, all of the block/bleed valves are connected into the E-stop button on the main control panel.  Note that the power to the safety system can only be turned off by a key lock to ensure the safety system is not inadvertently disabled.  There are also test buttons on the main safety control box to test all sensor relay systems for proper operation before each combustor startup.

**Figure 12: Main Box for Relays/Controls for Safety System**



**Figure 13: Main Control Panel in Control Room**
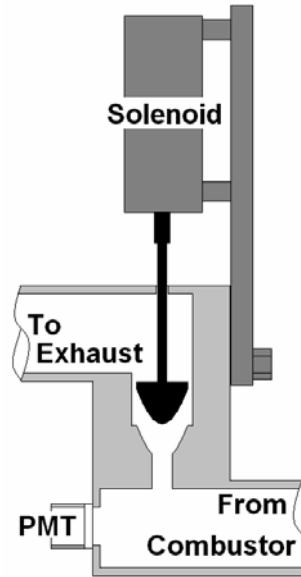
**Figure 14 Back-pressure controller**

*Back-pressure controlling system*

In order to ensure that the pressure in the combustor was held at a (approximately) constant pressure, a back-pressure controller was used. This controller used a pressure transducer located just upstream of the swirler and center body and proportions a plunger valve in the exhaust section to keep the right amount of pressure in the combustor. This plunger was controlled, up and down, by a computer through LabVIEW. Figure 14 is a cross-sectional view of the exhaust and shows how the plunger valve controls the back pressure of the combustor. The solenoid value shown is controlled from the computer.

## *ANALYSIS APPROACH*

This section describes the methods used to post-process the data and correlate blowout limits with the adiabatic flame temperature, laminar flame speed, Lewis number, and chemical time, parameters identified in the background section.

An internally developed code, "Happy Temperature", was developed to calculate temperature, heating value, and flame temperature. In addition, it can generate a matrix or list for syngas, which have the same heating value or adiabatic temperature, see **Figure 15.**
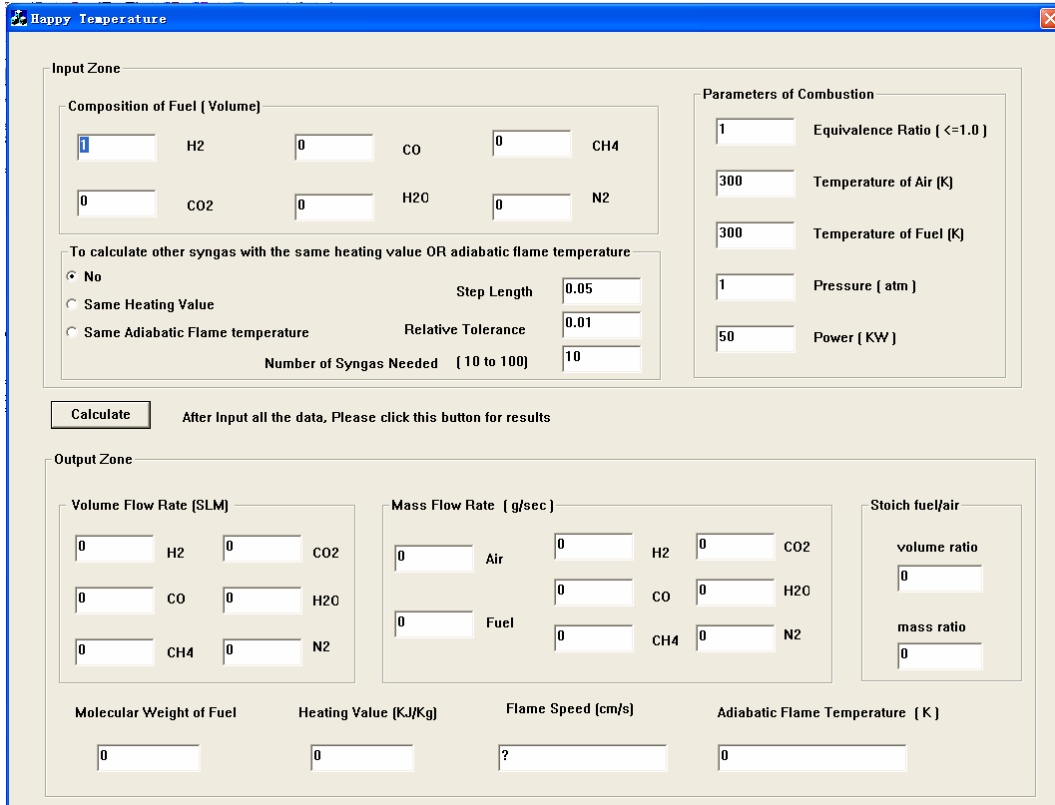
**Figure 15: Snapshot of Happy Temperature**

The mixture equivalence ratio is given by:

$$\phi = \frac{(Y_{Air}/Y_{Fuel})_{Stoic}}{Y_{Air}/Y_{Fuel}} \qquad (7)$$

where $Y_i$ is the mass of the indicated specie.

Adiabatic flame temperatures were calculated for a given mixture using standard methods. Laminar flame speeds were calculated with the PREMIX application in CHEMKIN, using the GRI3.0 mechanism. While this mechanism was primarily optimized for methane/air mixtures, good comparisons between its results and measurements have been obtained for a range of $H_2$/CO mixtures as well [29]. Chemical times were estimated using Eq. (1), where the thermal conductivity of the reactive mixture was determined using transport properties from TRAN in CHEMKIN and the equation[30]:

$$\lambda = \frac{1}{2}\left(\sum_{k=1}^{K} X_k \lambda_k + \frac{1}{\sum_{k=1}^{K} X_k/\lambda_k}\right) \qquad (8)$$

Diffusivity coefficients of a given species in the mixture were determined from:

$$D_{km} = \frac{\sum\limits_{j \neq k}^{K} X_j W_j}{\overline{W} \sum\limits_{j \neq k}^{K} X_j \Big/ D_{jk}} \qquad (9)$$

These diffusivity coefficients, combined with the mixture thermal conductivity were used to determine the Lewis number of the $k$-th specie:

$$Le_k = \frac{\lambda}{\rho C_P D_{km}} \qquad (10)$$

Since the above Lewis number is defined for a given species, not the mixture, a mixture averaged Lewis number was also determined using the relation:

$$Le_{mix} = \frac{\lambda}{\rho C_p \sum\limits_{k=fuel} A_k D_{km}} \qquad (11)$$

where $A_k$ is the percentage of heat release due to fuel $k$ relative to that of the entire mixture. We should emphasize that definition of the appropriate mixture averaged Lewis number is not trivial – analytical expressions derived using one-step kinetics and asympototics show that Lemix is not only a function of the Lewis number of the respective species, but also Zeldovich number[31].

In order to obtain the basic understanding of the properties of CO/$H_2$/$CH_4$ mixtures, a number of results showing the interdependence of these quantities are included below. Consider first the flame speed, $S_L$. Figure 16 illustrates the dependence of the flame speed upon fuel composition at two fixed adiabatic flame temperatures, 1500 and 2000 K. The fuel composition by volume is given by the location within the triangle, where the three vertices denote pure CO, $H_2$ or $CH_4$. At each point, the mixture equivalence ratio is adjusted such that the mixture has the given flame temperature. As expected, the high $H_2$ mixtures have the highest flame speeds. Note also the slightly higher flame speeds of the high $CH_4$ mixtures relative to those of CO mixtures.
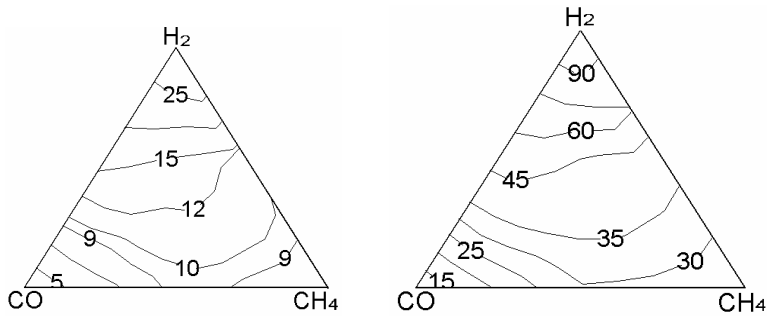
**Figure 16: Dependence of flame speed (cm/s) upon fuel composition at fixed 1500 K (left) and 2000 K (right) adiabatic flame temperatures with 300K reactants temperature.**

An alternative way to view these results is to plot adiabatic flame temperature at a fixed flame speed. This is done in Figure 17 for $S_{L,o}$=10 and 20 cm/s. Note the progression in flame temperatures from CO and $H_2$ mixtures being the highest and lowest, respectively.
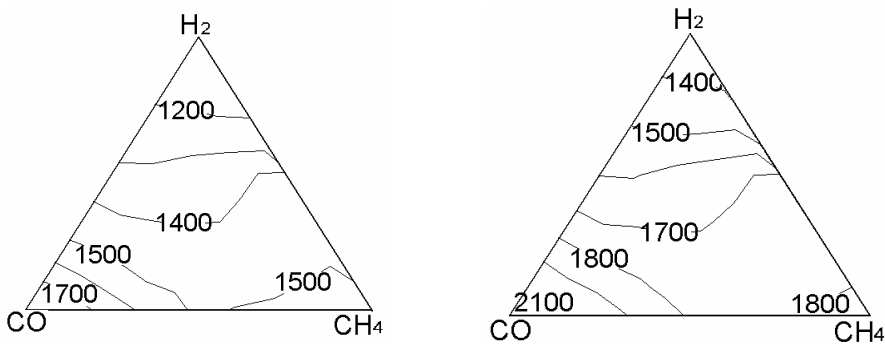


**Figure 17: Dependence of adiabatic flame temperature (K) upon fuel composition at fixed laminar flame speed 10 cm/s (left) and 20 cm/s (right) with 300K reactants temperature.**

Figure 18 plots the dependence of the mixture weighted Lewis number, $Le_{mix}$, upon fuel composition at a fixed flame temperature of 2000 K. As above, note that the mixture equivalence ratio is varying – it is the flame temperature that stays fixed. The figure shows that this Lewis number ranges from a low of 0.4 in the high $H_2$ mixtures to a high of slightly above one in the high CO mixtures.
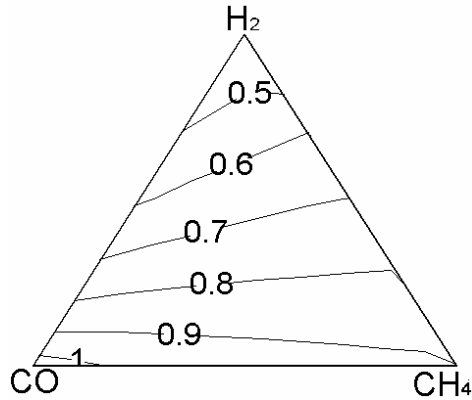
**Figure 18: Dependence of mixture weighted Lewis number, Le$_{mix}$, upon fuel composition at fixed adiabatic flame temperatures, 2000 K with 300K reactants temperature.**

Figure 19 plots the dependence of the chemical time, $\tau_{chem} = \alpha/S_L^2$ , upon fuel composition at a fixed flame temperature 1500K. Note the order of magnitude variation in chemical time from the fast $H_2$ mixtures to the slow CO mixtures.
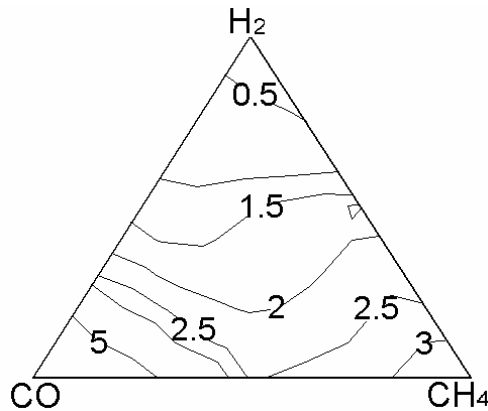


**Figure 19: Dependence of chemical time (ms) upon fuel composition at fixed adiabatic flame temperature, 1500 K.**

Kido and co-workers [32] have emphasized the significance of the relative mass diffusion rates of fuel and oxidizer, $D_{fuel}/D_{ox}$, over the Lewis number. However, there is nearly a one-to-one correspondence between these two dimensionless parameters for the mixtures considered here, as shown in Figure 20. This figure plots the dependence of $D_{fuel}/D_{ox}$ upon $Le_{mix}$ for a range of $H_2$/CO/ CH$_4$ mixtures. As such, in this report we only consider $Le_{mix}$, realizing that it is nearly

equivalent to mass diffusion ratios. $D_{fuel}$ is defined as heat-release weighted fuel diffusivity in the air, $D_{fuel} = \sum\limits_{k=fuel} A_k D_{k-Air}$ , and $D_{ox}$ is defined as oxygen diffusivity in the fuel and nitrogen.
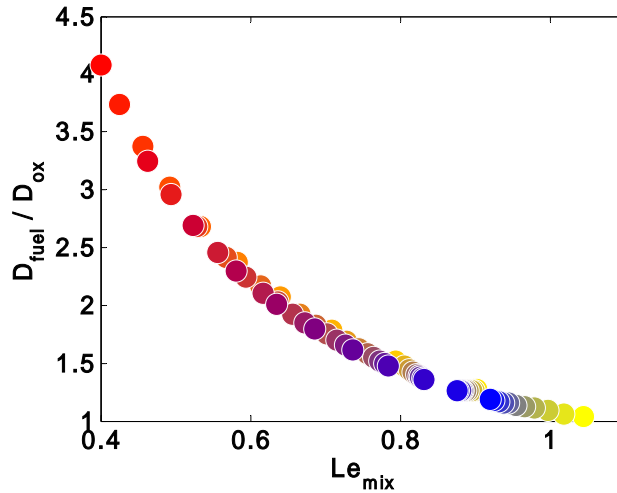


**Figure 20: Dependence of $D_{fuel}/D_{ox}$ upon mixture Lewis number.**

## *RESULTS AND DISCUSSION*

This section presents blowout results obtained during this report at two constant nozzle exit velocities: 59 and 39 m/s. This corresponds to combustor velocities (cold flow) of 6.0 and 4.0 m/s. Tests were performed at two pressure/temperature conditions: combustor pressure of 1.7 atm and 300 K reactants, and combustor pressure of 4.4 atm and 460 K reactants. The mean equivalence ratios ranged from roughly 0.15 to 0.60.

In order to facilitate presentation of results, we represent the mixture composition of $H_2/CO/CH_4$ by its color. Primary colors at the three vertices are used to represent each fuel constituent, where red, yellow, and blue denote $H_2$, CO, and $CH_4$, respectively. This is illustrated in **Figure 21**.
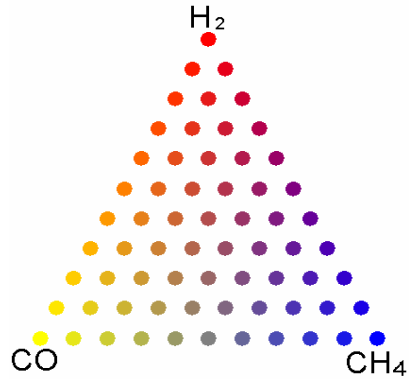
**Figure 21: Primary color mixing scheme used to denote fuel blend composition**

The basic test plan is to operate at uniformly spaced fuel compositions in $H_2/CO/CH_4$ space, such as is depicted in the figure above.

However, applying a uniform definition of blowoff is complicated by the fact that the manner in which the flame blew off varied with composition. In many cases, the blowoff event occurred abruptly with a small change in fuel composition, although sometimes preceded by slight liftoff of the flame from the burner. Defining the blowoff point was unambiguous in these instances; moreover, the point of blowoff and flame liftoff was nearly identical. This was the case for mixtures with mixtures with less than approximately 50% $H_2$ by volume. However, for high $H_2$ mixtures, the blowoff and liftoff events were quite distinct, see **Figure 22**. Usually, the flame became visibly weaker, lifted off from the holder, and moved progressively downstream with decreases in equivalence ratio before blowing off for good. As such, blowoff is defined in this report as the point where the flame is no longer visible in the 10.2 cm long optically accessible section of the combustor. Undoubtedly, this variation of liftoff/blowoff characteristics with fuel composition is responsible for some of the scatter in the experimental data. This point should be kept in mind when comparing 0-50% $H_2$ and 50-100% $H_2$ containing fuels.
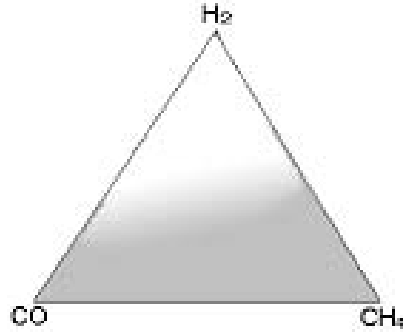
**Figure 22: Composition map describing regions where sharply defined blowoff event occurs (gray) and blowoff preceded by significant flame liftoff (white)**


These blowout limits were correlated with a variety of parameters. As noted in previous studies [17], the presence of $H_2$ has a strong impact on blowout limits of either $H_2/CH_4$ or $H_2/CO$ flames. **Figure 23**, which plots the dependence of the blowoff equivalence ratio upon the mole fraction of $H_2$ in the fuel, shows that $H_2$ also strongly affects the lean blowout limits of syngas mixtures ($H_2/CO/CH_4$), in spite of the complicated coupling chemical mechanisms among these species. It shows the well known result that, in general, mixtures can be stabilized with lower equivalence ratios as the $H_2$ concentration increases. However, note that the addition of small amounts of $H_2$ has small impacts upon blowoff limits and that the sensitivity of the blowoff equivalence ratio to $H_2$ level variations remains essentially constant across the entire range of $H_2$ levels. In other words, no discontinuous or steep drop in blowoff equivalence ratio was observed with small amounts of $H_2$ addition.

Besides at constant premixer flow speed, blowoff limits were also obtained at constant combustor power level (Figure 24), and constant burned combustor flow speed (Figure 25). These data also show that $H_2$ strongly affects the lean blowout limits of syngas mixtures.
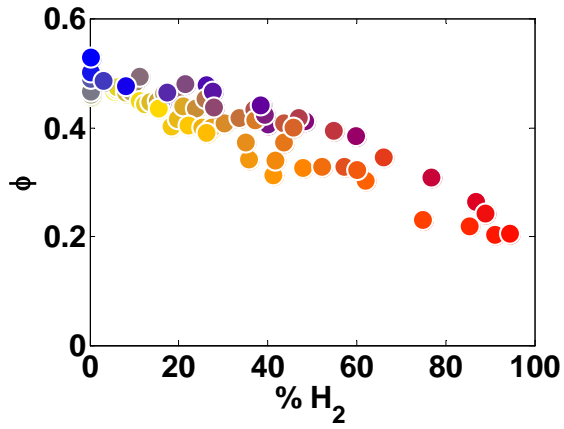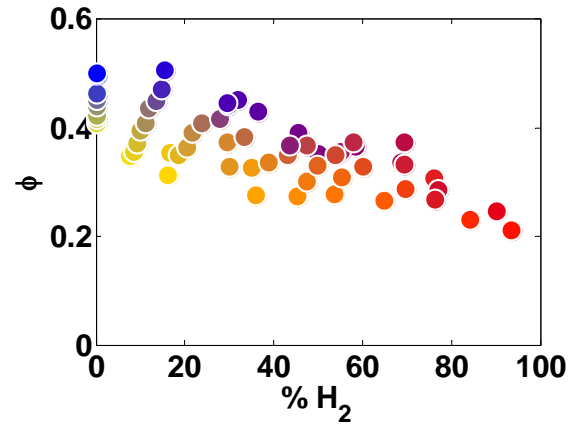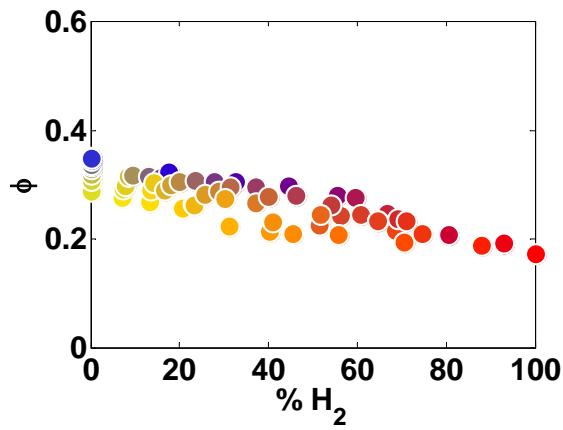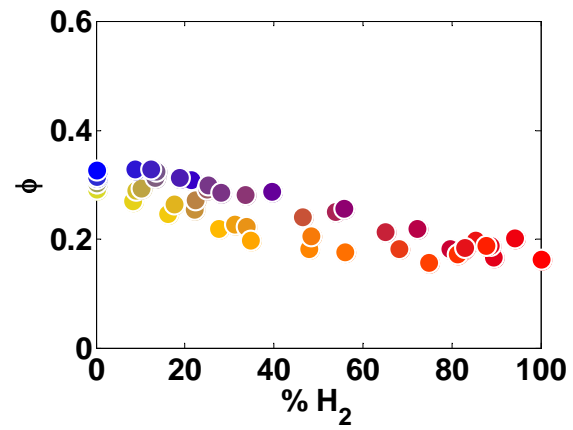
**Figure 23:** **Dependence of LBO equivalence ratio upon H₂ mole fraction at premixer flow velocities of 59 m/s at 300K reactants temperature and 1.7 atmospheres combustor pressure (a), of 39 m/s at 300K and 1.7 atmospheres (b), of 59 m/s at 458K and 4.4 atmospheres (c), of 39 m/s at 458K and 4.4 atmospheres (d).**
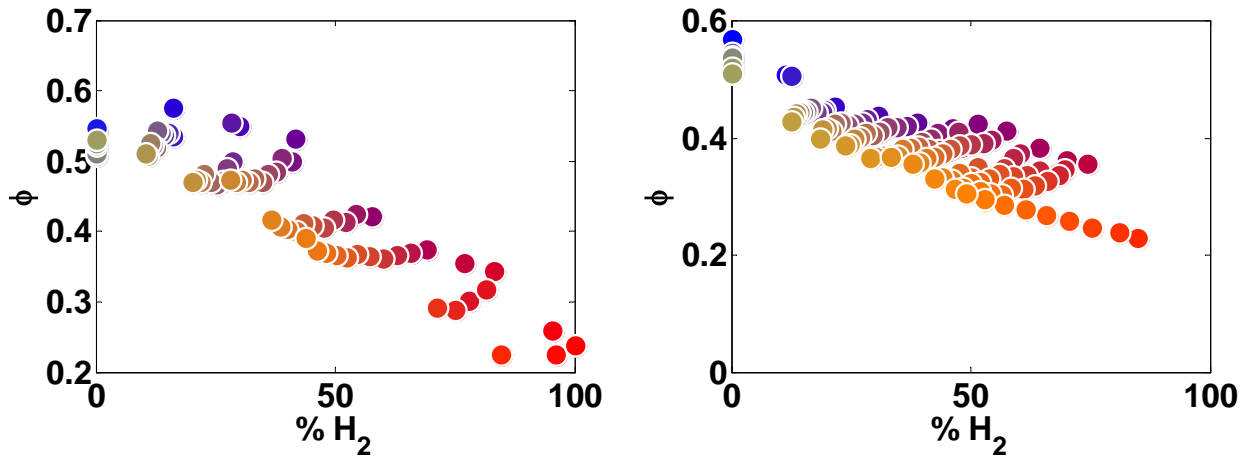
**Figure 24: Dependence of LBO equivalence ratio upon H$_2$ mole fraction at constant combustor power of 80kw (left), of 120kw (right) at 300K reactants temperature and 1.7 atmospheres combustor pressure.**
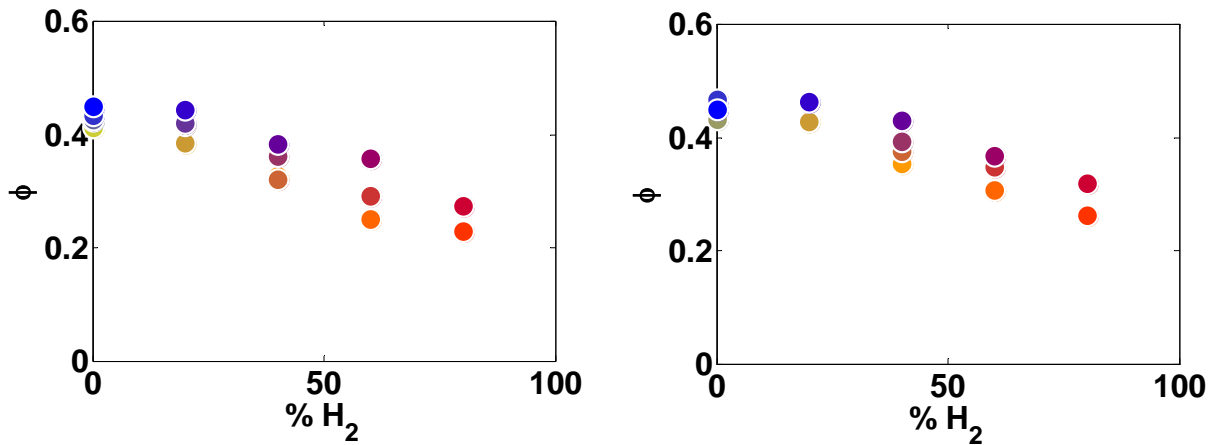


**Figure 25: Dependence of LBO equivalence ratio upon H$_2$ mole fraction at burned combustor flow velocities of 10 m/s at 300K reactants temperature and 1.7 atmospheres combustor pressure (left), of 17 m/s at 300K and 1.7 atmospheres (right),**

At one specific H$_2$ mole fraction, data scatters in a narrow band due to different ratios of CO and CH$_4$, and a higher ratio of CO/CH$_4$ makes the flames blowout in lower equivalence ratios,

although CO flame has a smaller flame speed or a large chemical time scale. It could be explained by the fact that $H_2$ has a stronger effect on CO than $CH_4$, or CO flame is much easier to be affected by the same amount of $H_2$ addition. **Figure 23** indicates that $CO/H_2$ flames are easier to blowout in a manner similar to $H_2$ flame than $CH_4/H_2$ flames. One possible reason is that $H_2$ supplies the OH radical pool, which plays a key role in CO oxidation, by the faster chain-branching reactions. Another possible reason is that CO has a higher adiabatic flame temperature which accelerates the overall reaction rate.
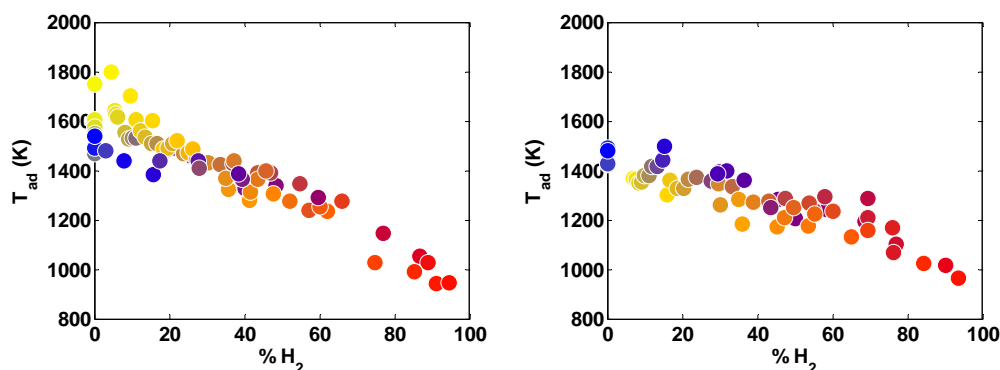


**Figure 26: Dependence of adiabatic flame temperature at LBO upon percentage of $H_2$; 59 m/s (Left) 39 m/s (right), both at 1.7 atmospheres**

Next, consider the dependence of adiabatic flame temperature at lean blowout upon the mole fraction of $H_2$. As shown in **Figure 26**, the data sets as a whole correlate well with these parameters. There is a nice trend between the percentage of $H_2$ and adiabatic flame temperature at lean blowout. That is, flames which have higher percentage of $H_2$ could stabilize at a lower adiabatic flame temperature. This could be partly explained by the chemical kinetics. The chain-branching reaction $H+O2 \Leftrightarrow O+OH$, which is very sensitive to flame temperature, plays an important role in such $H_2$ addition flames. For a given fuel composition, when the equivalence ratio decreases to some level where either flame zone temperature or the concentration of radicals is too low to maintain this chain-branching reaction, the local extinction or blowout happens. However, $H_2$ could provide more radicals for this chain-branching reaction, so that flames which have higher percentage of $H_2$ could stabilize at a lower adiabatic flame temperature. At one specific $H_2$ fraction, CO mixtures have a higher temperature level (more

obvious at low $H_2$ mole fractions in Figure 26 (a)). It is also noticeable that the adiabatic flame temperature is more sensitive to the percentage of $H_2$ for the higher flow speed case due to the overall higher stretch rate it has.

Similarly good correlations between the laminar flame speed, Lewis number, and a number of other combustion parameters at blowoff upon $H_2$ level were observed. This brings us to an important point that must be recognized in extracting an understanding of the blowoff physics from these correlations. First, blowoff limits are clearly a strong function of $H_2$ levels. Second, many other parameters, such as diffusivities, flame temperature, etc. are also strong functions of $H_2$ level. *As such, it is important to not draw conclusions about blowoff physics only because one can correlate results with parameters that are simply functions of the $H_2$ percentage.* For example, a very nice correlation between $T_{ad}$ vs. $Le$ at blowout exists, because both of them are functions of percentage of $H_2$. In other words, regardless of whether the mixture $Le$ is a physically meaningful parameter, a good correlation will still be observed. In some sense, this is analogous to correlating $T_{ad}$ vs $2*T_{ad}$ at blowoff – obviously, a perfect correlation is observed, regardless of whether this is a physically significant parameter.



(a)  (b)
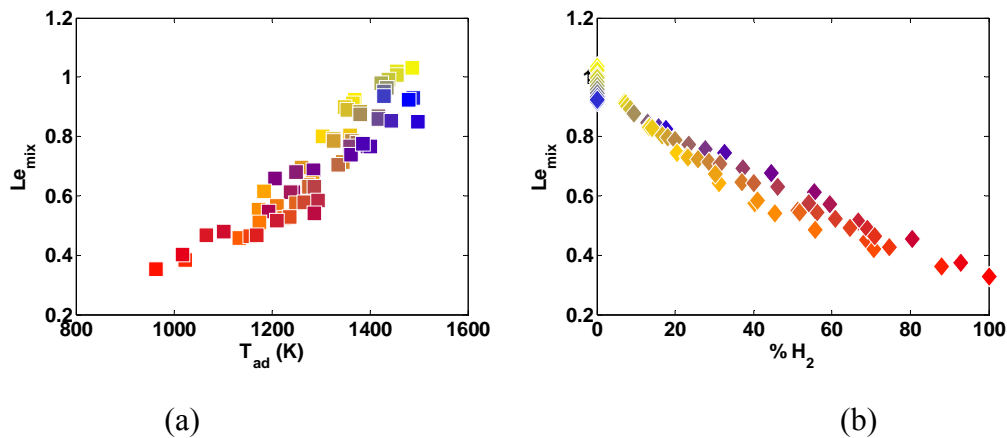
**Figure 27: Dependence of Lewis number (a) upon adiabatic flame temperature at LBO at 4 m/s 1.7 atm (b) upon percentage of $H_2$ at 59 m/s 4.4 atm**

For example, Lewis number of the mixture, $Le_{mix}$, is a key parameter for the flame instability or flame propagation for stretched flame or turbulent flame, so using $Le_{mix}$ to correlate the lean blowout data is reasonable and meaningful. Now, consider correlating these blowout results with

Lewis numbers, $Le_{mix}$, see Figure 27 (a). The correlation is quite good in all instances, although only one result is shown. However, in light of the comments in the last paragraphs of this section, some care must be taken in placing too much emphasis on this point, as the Lewis number is very closely related to the $H_2$ percentage, Figure 27 (b). A perfect linear relation exists between $Le_{mix}$ and percentage of $H_2$. This is because the diffusivity of $H_2$ is much larger than that of CO or $CH_4$, so percentage of $H_2$ dominates the $Le_{mix}$.



(a)                                                  (b)
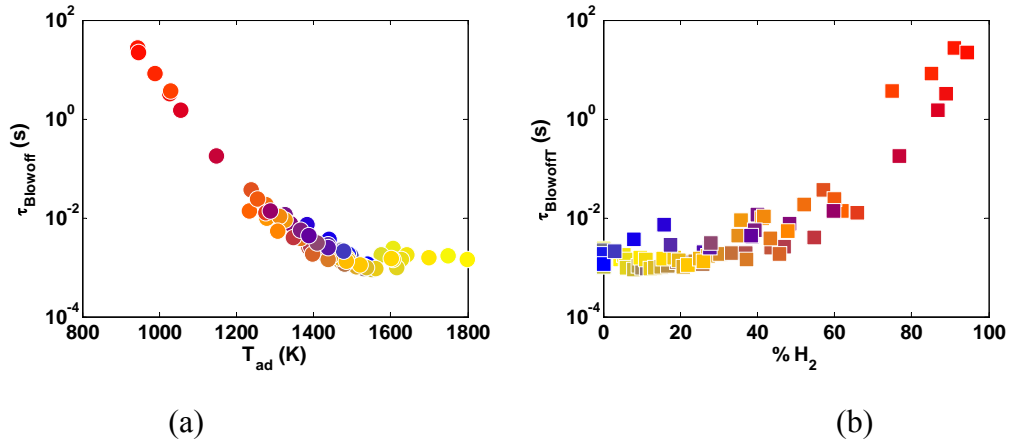
**Figure 28: Dependence of blowoff residence time (a) upon adiabatic flame temperature at LBO, 6 m/s (b) upon percentage of $H_2$ at 4 m/s , both at 1.7 atm**

While chemical time based correlations, such as described in the Background section, have been used successfully in a number of prior studies for narrow fuel range variations, we have not found them very successful in correlating our data. Since these experiments were performed at fixed unburned gas temperature and velocity, the arguments in the context of Eq. (2) suggest that the "loading parameter" should then only be a function of burned gas temperature and chemical time. However, at some lean mixtures where stable flames were observed, we were unable to get PREMIX to converge, so blowoff residence time, $\tau_{Blowoff}$ , is used here to scale chemical time. As shown in Figure 28 (a), it is noticeable that there are two parts of the correlation curve; one is that adiabatic flame temperature, $T_{ad,}$ greater than 1300K where $\tau_{Blowoff}$ changes slowly with $T_{ad}$, and the other part is that $T_{ad}$ less than 1300K where $\tau_{Blowoff}$ changes greatly with $T_{ad}$. These two parts have the counterparts in Figure 28 (b), 0-50% $H_2$ and 50-100% $H_2$. Considering the different definitions of blowout for these two parts in the previous section, it is necessary to analyze these data separately.
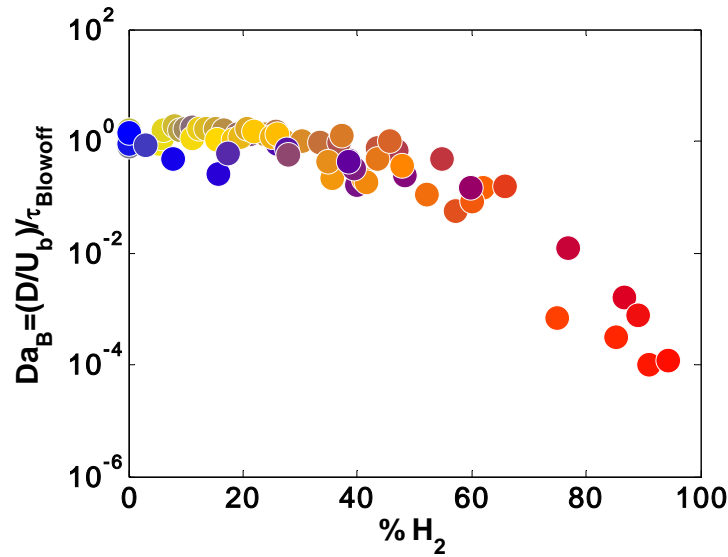
**Figure 29: Damköhler numbers of mixtures at constant premixer flow speed of 59 m/s at 300K reactants temperature and 1.7 atm combustor pressure.**

Damköhler (*Da*) number correlations were found to correlate the data over all flow velocities, pressures and temperatures for all mixtures with $H_2$ levels below 50%, as shown in **Figure 29**. In the plot, the reference length scale, *D*, was the combustor width, 5.1 cm. Damköhler numbers were evaluated using both the unburned, $Da_U$, and burned flow speed, $Da_B$, as reference velocity scales. Utilizing the burned gas speed resulted in slightly better ability to correlate the data, as reflected in slightly lower errors (about 10 %) in predicted blowoff equivalence ratio, $\delta\phi_{rms}$ (described below), and so is used for these results. **Figure 29** shows that blowout occurs at a nearly constant *Da* for these composition values (although

**Figure 29** was plotted in *logarithm* scale, $\tau_{Blowoff}$ is an exponential function of equivalence ratio). At the same time,

**Figure 29** also shows that a constant *Da* correlation is inadequate for describing blowout limits of higher $H_2$ level mixtures. It is possible that this is simply a reflection of the fact that the blowout process changes with $H_2$ levels and that our "blowoff definition" is not the most physically meaningful, see discussion of **Figure 22**. For example, perhaps identifying the point where the flame first lifted off the flame holder would have been more useful.

41

A second possibility for this change in blowoff *Da* value shown in **Figure 29** may be due to preferential diffusion effects, a consideration that has also been used to scale changes in turbulent flame speed of mixtures whose constituents have significant variations in diffusivity. One approach for incorporating these effects is to note that the local equivalence ratio changes along the wrinkled flame, being both higher and lower than the average at different spatial locations. Kido and co-workers [33] suggested correlating mixture turbulent flame speeds by utilizing mixture properties at an adjusted equivalence ratio, $\phi_{adj}$; i.e., not at the average equivalence ratio, $\phi_{ave}$, but the average value plus some $\Delta\phi$. As such, mixture properties are correlated at $\phi_{adj}=\phi_{ave}+\Delta\phi$. They suggest the following relation for $\Delta\phi$, based upon empirical fits of their data:

$$\Delta\phi = C * \ln(D_F / D_{OX}) \qquad (12)$$

where $D_F$ and $D_{OX}$ denote the mass diffusivity of fuel and oxygen, respectively, and *C* is an empirical constant whose value they suggest as 0.3.

We found that utilizing a value of *C* close to 0.1 gives a nearly constant blowoff Damköhler number for all of our data sets, **Figure 30**. This plot shows that blowoff occurs at a nearly constant value of local Damköhler number, where the $\tau_{Blowoff}$ is estimated at the equivalence ratio $\phi_{adj}=\phi_{ave}+\Delta\phi$. In this case, the best value for *C*=0.07 and the average value over all the test points of $\overline{Da_B}$, at blowoff is 0.2. **Table 1** summarizes the results from the other two tests by presenting the best fit value for *C* for each individual data set and the corresponding $\overline{Da_B}$ value. It can be seen that $\overline{Da_B}$ does vary somewhat with each data set, but is always an O(1) quantity.

In order to quantify the scatter in the correlations shown in the table and the capability for actually inverting the above procedure to be used as a blowoff prediction methodology, we employed the following procedure. Assume that the equivalence ratio at blowoff is now the unknown and must be predicted, $\phi_{LBO,pred}$. Assume also that the Damköhler number at blowoff is known and equal to the value $\overline{Da_B}$ compiled in the table. We then solve the following implicit equation for $\phi_{LBO,pred}$ for each fuel composition:

$$\overline{Da_B} = \frac{d}{U_b \tau_{Blowoff}(\phi_{LBO,pred} + C\ln(D_F/D_{ox}))} \qquad (13)$$

This procedure is repeated for each fuel composition.  In general, $\phi_{LBO,meas}$ and $\phi_{LBO,pred}$ are not identical, and so the root mean square (rms) of their difference over all the data points is referred to as $\delta\phi_{rms}$.  The table also compiles the values of $\delta\phi_{rms}$.  As can be seen, assuming a constant Damköhler number at blowoff results in a capability for predicting the equivalence ratio value to within about 0.02 - 0.04.

| Test group | Best Fit $C$ Value | | |
|---|---|---|---|
| | C | $\overline{Da_B}$ at $\phi_{adj}$ | $\delta\phi_{rms}$ |
| T=300 K  P=1.7 atm $U_0$=59 m/s | 0.1 | 2.1 | 0.04 |
| T=300 K  P=1.7 atm $U_0$=39 m/s | 0.08 | 1.1 | 0.03 |
| T=458 K  P=4.4 atm $U_0$=59 m/s | 0.07 | 0.2 | 0.02 |

**Table 1: Summary of optimum model constants for correlating blowoff data and resulting scatter in fitted data.**

Moreover, due to the exponential dependence of $\tau_{Blowoff}$ upon equivalence ratio, varying the precise value of $\overline{Da_B}$ or C does not substantially impact the errors in $\phi_{LBO,pred}$.  For example, in the first case above, assuming blowoff occurs at constant values of $Da$=1.0 or 3, instead of the best fit value of 2.1, results in $\delta\phi_{rms}$ =0.045 and 0.043, respectively.

Moreover, both $T_{in}$=300K, $P$= 1.7 atm data sets can be reasonably collapsed with a single $\Delta\phi$ equation or $C$ value.  To illustrate, **Figure 31** compares the predicted and actual blowoff equivalence ratios for all low temperature data taken in this study, assuming $C$=0.1 and $\overline{Da_B}$=1.7. It can be seen that the error in $\phi_{LBO,pred}$ is generally less than 0.05, and $\delta\phi_{rms}$ = 0.045.  Moreover, the highest errors are encountered with the very high CO mixtures, which may simply be a manifestation of the sensitivity of high CO mixtures to ambient humidity levels and other factors influencing H levels.  If the P=4.4 atm, T=460 K data set were also plotted, they would also cluster along a line, but with a systematic difference from the grouping in this graph.,  In other words, the optimum model constants (particularly the C value) vary with operating conditions.
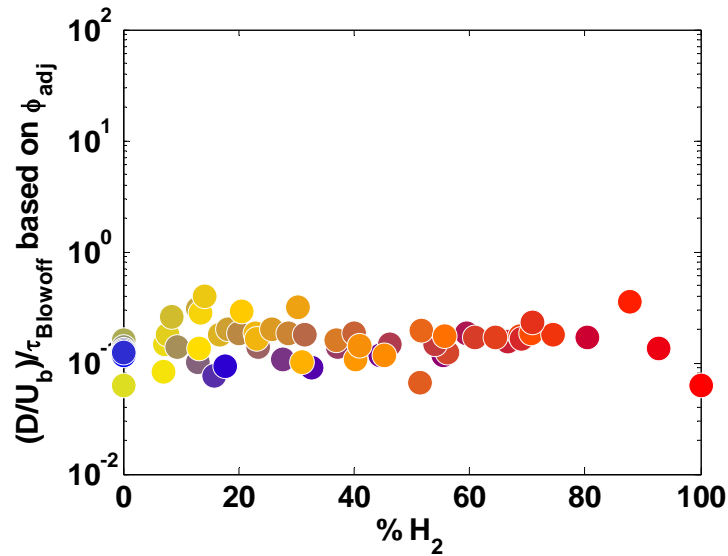
**Figure 30: Damköhler numbers of mixtures based on local equivalence ratio at premixer flow velocities of 59 m/s at 458K reactants temperature and 4.4 atm combustor pressure.**

There are a variety of reasons that the remaining scatter could be present, such as inherent noise in the blowoff equivalence ratio. In addition, other more subtle factors, such as reference length and reference flow velocity could easily change somewhat with approach flow velocity.

We should emphasize that the $C$ value in the $\Delta\phi$ calculation was chosen *empirically* to give the best fit. Although the *Da* mechanism, considering preferential diffusion effects, could correlate and predict the lean blowout limits very well, the real physical meaning behind these correlations are still uncertain and require further study.
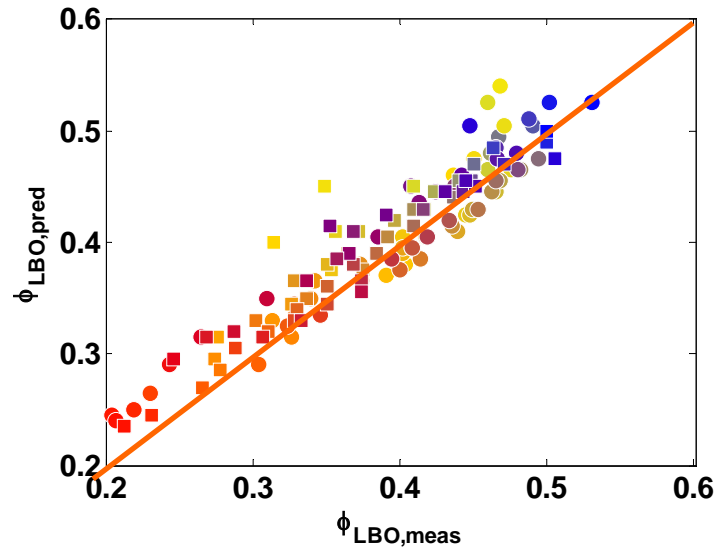
**Figure 31: Comparison of predicted and measured blowoff equivalence ratio for all T=300 K, p = 1.7 atm data.  circle:**$U_0$**= 59 m/s, square:** $U_0$**= 39 m/s.**

# 7. DYNAMIC PHENOMENOLOGY OF LEAN BLOWOFF

## *BACKGROUND*

In the previous section, it was noted that the phenomenology of blowoff changed markedly with $H_2$ levels in the fuel, see discussion of **Figure 22**. For lower $H_2$ mixtures (~<50% $H_2$ by volume), the blowoff event occurred abruptly and was precipitated by a small reduction in fuel/air ratio (although sometimes preceded by slight liftoff of the flame from the burner). However, for high $H_2$ mixtures, the flame liftoff and blowoff events were quite distinct. Furthermore, as the mixture approached blowoff, the flame becoming visibly weaker, lifted off from the holder and moved progressively downstream. Finally, it was noted that the definition of blowoff at these very high $H_2$ levels was somewhat arbitrary and very much a function of the definition of "blowoff".

The objective of this task was to follow up on these observations and systematically characterize the blowoff phenomenology as a function of the $H_2$ levels in the fuel. This was accomplished through high speed visualizations of the flame emission and velocity field measurements. The dynamic blowoff process of methane flames has been studied and characterized in different stabilization mechanisms, pilot, bluff body, and swirling flow[34,35,36,37]. In the swirling flame, it has been showed that the swirling flame tends to oscillate between extinction and reignition phases [36,37]. The flame is stabilized by the inner recirculation zone (the vortex breakdown bubble), and locally extinguishes/reignites under near blowoff conditions. The number of extinction/reignition events per unit time monotonically grows as blowoff is approached. These observations have formed the basis of an active control system that detects blowoff precursors and applies closed loop active control to prevent its occurrence [37]. Our objective in this task was to generalize the study of the dynamic blowoff process of a methane flame to flames with varying levels of $H_2$ dilution. It should be emphasized that this blowoff phenomenology is geometry dependent and is a function of, for example, the degree of constriction of the exhaust nozzle. As such, we took special effort to perform this study on a well characterized burner that is identical to studies performed at Sandia National Laboratory.

## *EXPERIMENTAL SETUP*

**Combustor and Flow System**

For this task, we duplicated an experimental rig developed at Sandia National Laboratories by Dr. Bob Schefer and Joe Oefelein to capture chemiluminescence and visualize the flame front and flow field. This was done in order to have a similar test facility to facilitate comparisons of data and simulations. This gas turbine simulator is an atmospheric pressure, premixed, swirling stabilized dump combustor, which is the basic configuration of most gas turbine combustor. The combustor is shown in **Figure 32**.

The facility consists of a swirler/nozzle, combustor, and exhaust sections. Premixed gas, consisting of $H_2/CH_4$ mixtures and air flows through a swirler housed swirler/nozzle section. The nozzle is an annular tube with inner diameter of 28mm. The center body has an outer diameter of 19 mm. The overall flow area remains constant at 3.0 cm$^2$ inside the nozzle. Tests were performed with a six-vane, 45$^o$ swirler, which is located in the annulus between the centerbody and nozzle wall, see **Figure 33**. The theoretical swirl number, which is 0.85, is calculated by [38],

$$S = \frac{2}{3}\left[\frac{1-(d_h/d)^3}{1-(d_h/d)^2}\right]\tan\theta \quad (14)$$

where $d_h$ and $d$ are the diameters of centerbody and swirler, respectively, and $\theta$ is the swirler vane angle. The fuel is injected 150 cm upstream of the combustor to achieve a premixed condition. The combustor consists of a 305 mm (12 inches) long quartz tube, which permits the detection of ultraviolet (UV) radiation and imaging. The quartz tube has an inner diameter of 115 mm and rests in a circular groove in a base plate. An adapter slides in four standing bars, sitting on the top of the quartz tube, and the exhaust nozzle is connected to the adapter. The exhaust nozzle has a 127mm contraction section with the area ratio 0.44, and a chimney section which is 102mm long with inner diameter of 51mm.
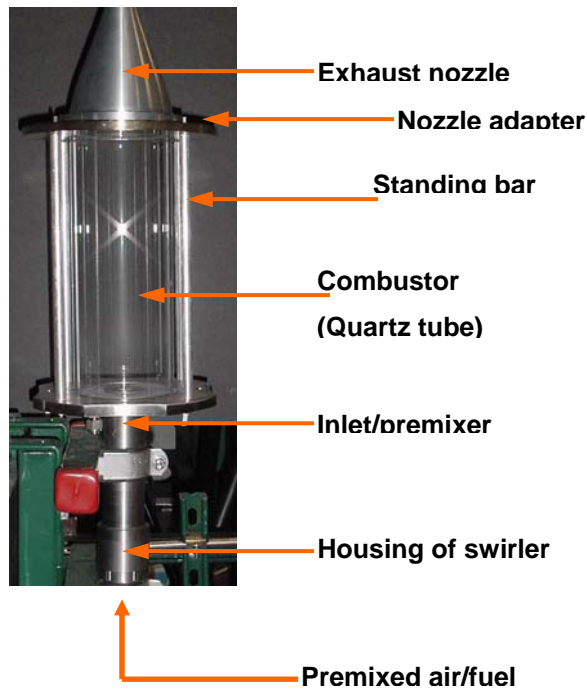
**Figure 32: Photograph of the combustor facility**

**Figure 34** shows the schematic diagram of the flow control system. High-pressure natural gas and air are supplied from building facilities. The hydrogen is supplied from bottles. The air and fuel flow rates are measured with a flowmeter and mass flow controllers (MFC's), respectively. The same fuel mixing facility in the previous section was used to generate the syngas mixtures ($H_2$/CO/$CH_4$). Both the flowmeter and MFC's were calibrated using the specific gas with which they were to meter. The maximum resultant uncertainty in the flow rate measurements is 5% of full scale, and in blowoff equivalence ratios is 0.01-0.02 for most of the cases. The largest uncertainty in $\phi$ of 0.03 occurs with pure $CH_4$. The air is choked before the mixing section, and the premixed air/fuel is choked again inside the inlet tube of the combustor (not shown) upstream of the swirler to minimize the impact of perturbations in the combustor impacting the fuel/air mixing process.
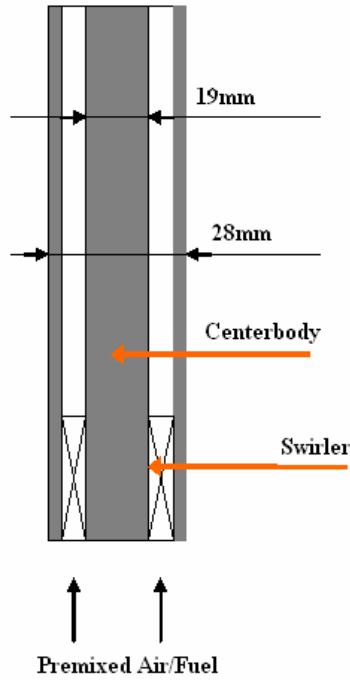
**Figure 33:  Cross section of inlet/premixer assembly**
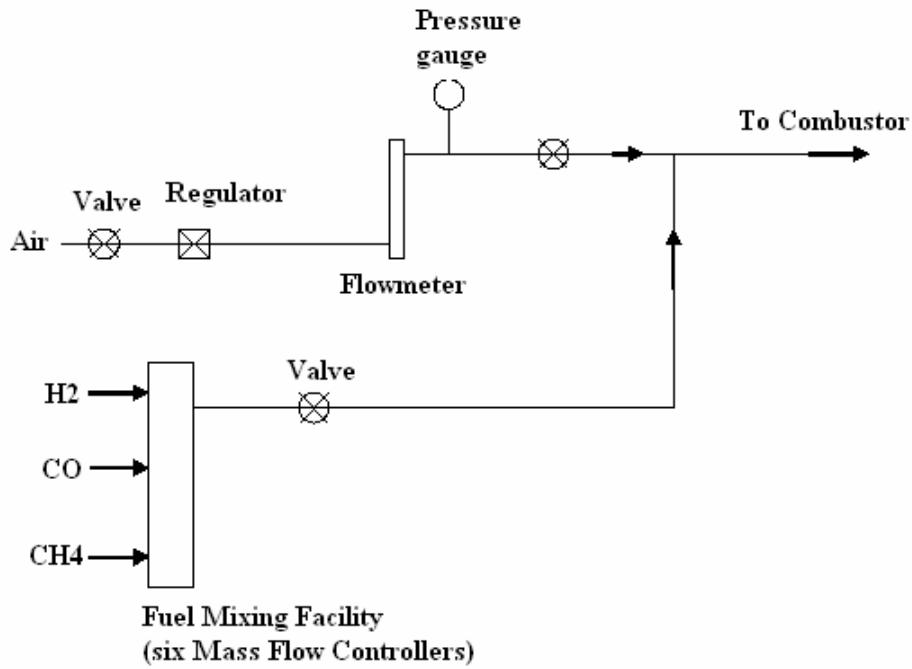


**Figure 34: Schematic diagram of the flow control  system**

## Diagnostic methods and Instrumentations

To help understand the dynamic processes of lean blowoff for syngas mixtures, several types of instrumentations and diagnostic methods were employed in this study.

### *High Speed Visualizations and OH chemiluminescence*

High speed visualizations of the flame were obtained with an Ultracam3, Gen III intensified camera at 1000 frames/sec and 512 x 512 resolution. The photocathode is sensitive to light in the 400-900 nm spectral region and is, thus, unfortunately insensitive to the UV light that constitutes the primary chemiluminescence emission for high $H_2$ flames. As such, this variation of camera sensitivity should be kept in mind when comparing the images with varying $H_2$ levels in the images below.
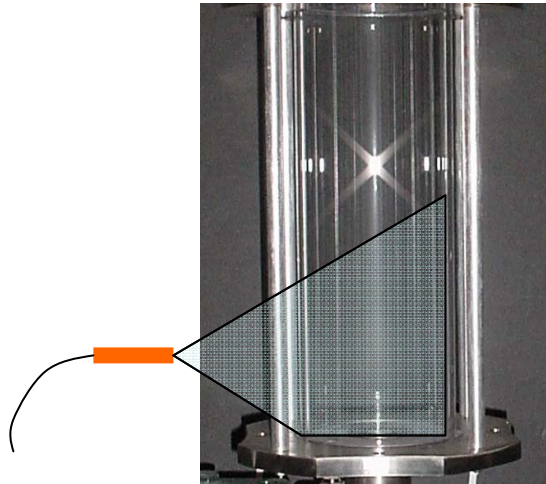


**Figure 35: Location of the optical probe**

In addition, UV radiation from the high $H_2$ flames was monitored with an optical fiber bundle (NA=0.44), with the head located 46 mm above the dump plate of the combustor and 171 mm radially from the combustor centerline, see **Figure 35.** This volume was placed such that light is collected from the IRZ (inner recirculation zone). The light passes through an interference filter centered at 308 nm and with a full-width-half-maximum (FWHM) of 10 nm, which corresponds to the primary spectral region of OH* emission. This radiation was detected

by a miniature, metal package PMT (Hamamatsu H5784-04). This PMT has a built-in amplifier (bandwidth of 20 kHz) to convert the current to voltage and operates from a 12 VDC source.

The signal output from the sensors was low pass filtered by a Krohn-Hite Model 3362 digital Butterworth filters and then fed into a National Instruments A/D board. The sampling frequency was 2 kHz. The low pass filter frequency (for anti-aliasing) was set at half the sampling frequency, 1 kHz.


### *PIV system*

The velocity field in the combustor was measured using Particle Image Velocimetry (PIV) as explained by Raffel *et. al.* [39]. The system consists of a dual head Nd:YAG laser, a high resolution CCD camera, a mechanical shutter and a centralized timing generator orchestrating the activation of each component. In addition a cyclone seeder built in-house was used to supply anhydrous aluminum oxide ($Al_2O_3$) with an average particle size of 3μm.

Each laser head delivered a 120 mJ/pulse beam at a wavelength of 532 nm. The beams passed though sheet forming optics, consisting of a convex spherical ($f = 1$ m) and a convex cylindrical lens ($f = 25.4$ mm), resulting in a 500 μm thick light sheet at the center of the combustor. The CCD camera captured the images of the illuminated particles at a resolution of 1600 x 1200 pixels (corresponding to 76 mm x 102 mm) in frame straddling mode. This allowed for the duration between the laser shots to be at the desired level of 10 μs. In addition the camera was also fitted with a 532 nm laser line filter with a FWHM of 3 nm to restrict any background noise.

The images were processed using the DaVis software package, provided by LaVision Inc. This software uses an adaptive algorithm to obtain the velocity field. The grid size was 32 pixels x 32 pixels with a 50% overlap. The blue dashed line **in Figure 49** (a) illustrates the interrogation volume for the PIV measurements shown in this report.

One of the most significant errors present in PIV measurements in a swirling flow comes from out of plane motion of the flow which causes particles to exit and enter the interrogation volume between successive laser shots. The laser sheet thickness, the duration between laser shots, and the seed density have been carefully optimized to minimize this error. Assuming an overall 5 m/s tangential velocity, the distance traveling between two laser shots is 50μm, which

is 10 percent of the laser sheet thickness at the center of the combustor. We estimate that the velocity uncertainties to be on the order of 5% [17,**Error! Bookmark not defined.**].

## *RESULTS AND DISCUSSION*

**OH Chemiluminescence**
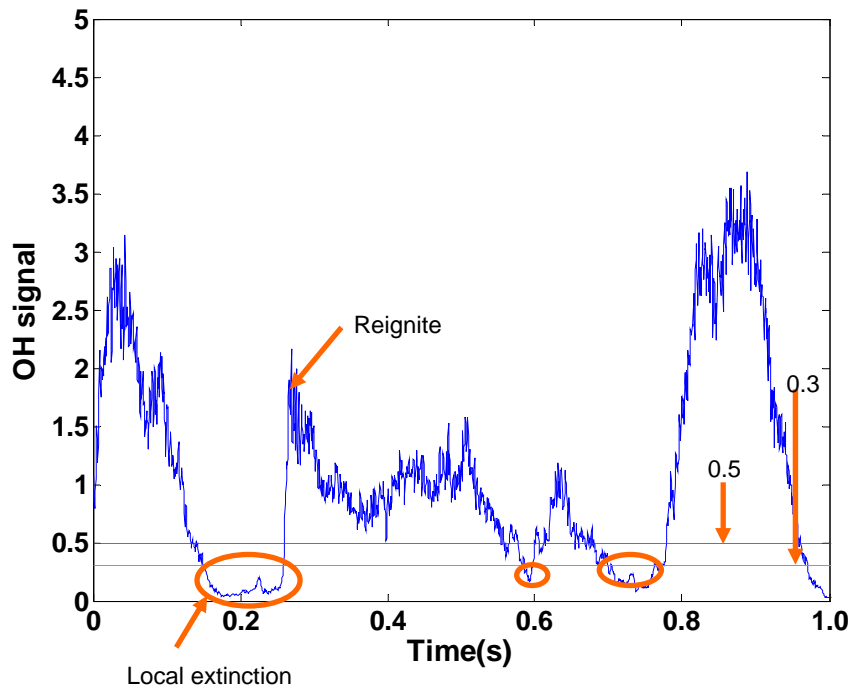


**Figure 36: Time series data of OH signal of extinction-reignite events**

**Figure 36** shows the OH chemiluminescence signal from an optical probe which was focused at the inner recirculation zone, see **Figure 35**. Because the level of chemiluminescence signal is determined by the power of the flame, which is varying with equivalence ratio, the OH signal is normalized by its mean value. Local extinction is defined when the intensity of the signal drops lower than some threshold, and ends when the signal goes above this threshold. However, sometimes during a local extinction the signal oscillates above and below the threshold. As such, a second threshold was defined a little higher than the first threshold to make

sure that this is only counted as one event. For this example, 0.3 and 0.5 were used as the first and second thresholds for local extinction. Data in **Figure 36** was collected at an equivalence ratio of 0.50 for the $CH_4$/Air flame. It can be seen that unsteady events are characterized by an almost complete loss of chemiluminescence signal quickly followed by a strong signal spike. This corresponds to a local extinction of the flame followed by a strong reignition of the flame. The local extinction events were circled in this plot. These distinctive extinction and reignite span a period from O(1s) to O(0.001s), without any obvious periodicity or frequency prior to lean blowout. **Figure 37** shows the power spectral density of the signal for equivalence ratios of 0.6, 0.5, and 0.46(lean blowout occurred at an equivalence ratio of 0.45 in this set of experiments). There are no peaks arising in the low frequency range as LBO limit is approached. This indicates that there are no coherent, periodic oscillations occurring near the blowout limit. The only obvious peak is at 250 Hz, which is related to the natural frequency of the combustor.
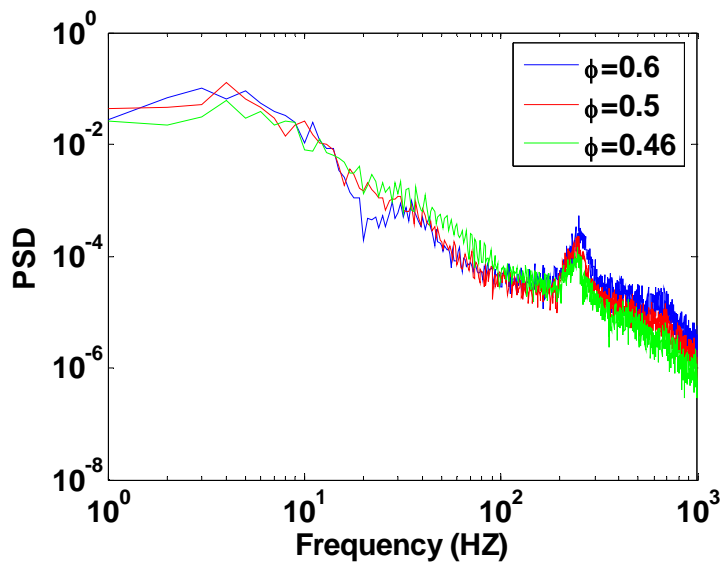


**Figure 37: Power spectral density (PSD) of OH signal of $CH_4$ flame at different equivalence ratios**

As the LBO limit is approached, more of these events occur in a given time period and thus the time between two such events decreases. **Figure 38** shows the dependence of the number of events per second on the equivalence ratio for five kinds of syngas. The data shows that flames can be stabilized at lower equivalence ratios with increasing $H_2$ percentage. When the flame is approaching the lean blowout, the number of events increased greatly. It shows that

more events are observed prior to blowout with higher percentages of $H_2$- this illustrates the enhanced robustness of these flames to blowout. More events means that the flame undergoes extinction events more frequently and undergoes a longer time in the extinction phase. As a consequence, the flame has a shorter and shorter time to reignite and sustain itself. This phenomenon may be explained by the difference of chemical time for these mixtures. The chemical time of $H_2/CH_4$ flame decreases with the increasing of $H_2$ percentage - so a higher level $H_2$ flame can stand a shorter time to reignite.
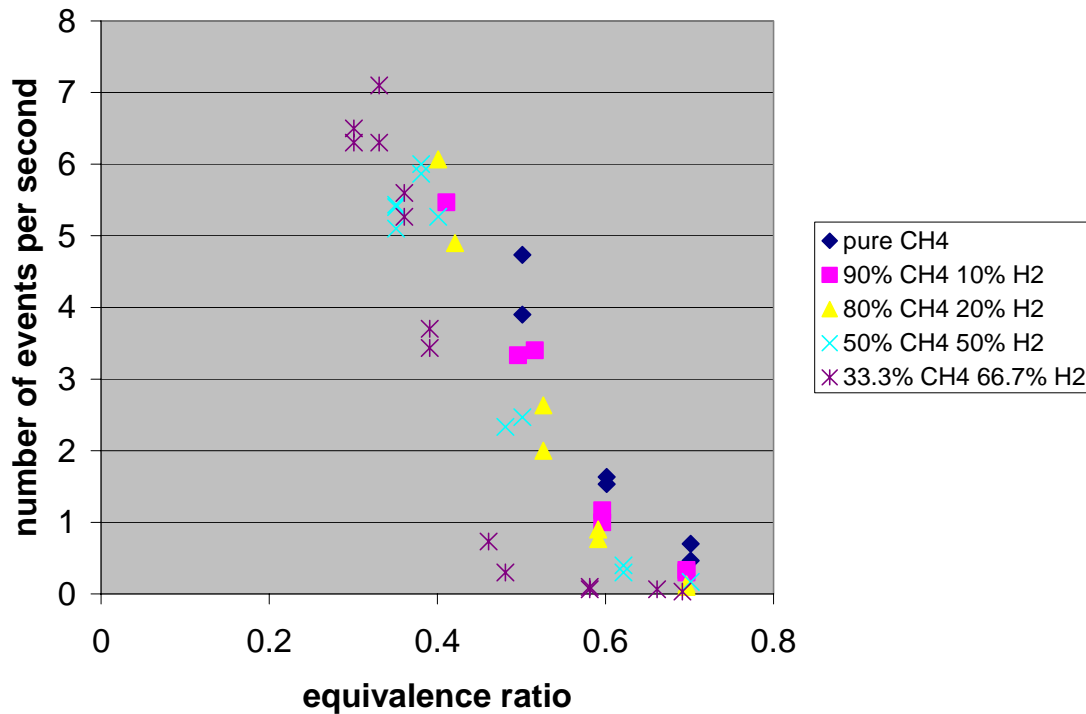


**Figure 38: Dependence of events numbers upon equivalence ratio for different fuels**

**High Speed Images**

This section describes the dynamics of near blowoff flames. Tests were performed at room temperature, atmosphere pressure, and constant nozzle exit velocity of 29m/s.

A qualitative stability diagram of $H_2/CH_4$ mixtures is shown in **Figure 39**. The regimes are differentiated by visual observation. For a given fuel composition, as we move vertically down the chart by reducing fuel/air ratio, at some point a certain level of "enhanced unsteadiness" becomes evident, indicated by the upper dashed line. For low levels of $H_2$, further

reductions in fuel/air ratio cause blowoff, indicated by the lower solid line. At higher levels of $H_2$, an additional flow regime, associated with a columnar flame zone is also present. This columnar region will be discussed later in this report. The four solid circle points represents the four cases studied in detail in this report. Note that there is a monotonic reduction in blowoff equivalence ratio with increasing $H_2$ levels, consistent with prior section (task 2).
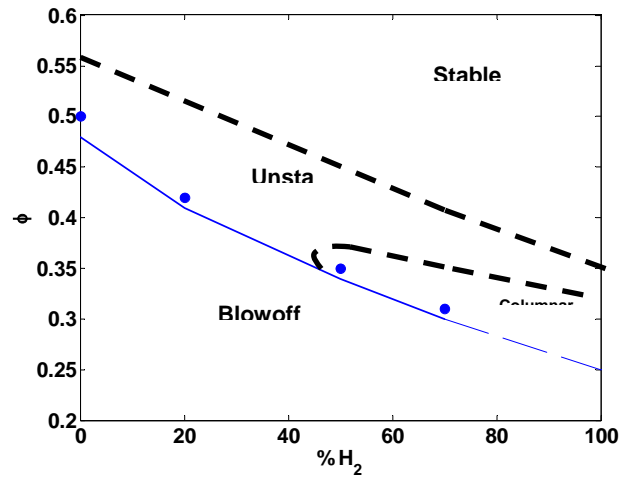


**Figure 39: Diagram of flame stability with different $H_2$ addition levels.**

To provide a baseline, a set of stable flame images are provided in **Figure 40**, which shows chemiluminescence gray scale image (intensity based coloring code) at an equivalence ratio of 0.56. The definition of equivalence ratio is based on the overall fuel mixture. We should note that these colorized images are difficult to interpret if viewed in grayscale. The boundary of the images corresponds to the combustor walls. A compact V shaped flame[2] stabilizes slightly downstream of the nozzle exit. There are minimal reactions at the two corners between the combustor wall and the dump plate, where the flow is recirculating (referred to here as the Corner Recirculation Zone, CRZ).

---

[2] This V-shape is not obvious from these images due to the integration of light intensity over the line of sight, but very obvious from direct visualizations.
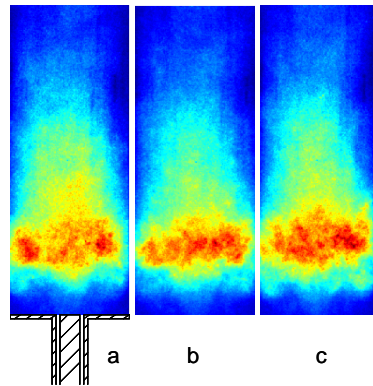
**Figure 40: Consecutive images of stable CH₄/Air flame (φ =0.57; images separation =10ms)**

A typical extinction/reignition process for a natural gas flame near blowoff is shown in **Figure 41**, at an equivalence ratio of 0.5. Moving from (a) to (g), the flame gradually weakens in intensity, particularly about half way up the image in the axial direction. In addition, it lengthens axially, reverting from a more compact region in (a) to an axially distributed region in (d) and (e). In images (f) and (g), the axially distributed flame appears to split into two sections, with hardly any radiation evident from the center. This region reignites in images (h)-(j) which leads to a more axially uniform, but axially compact intensity distribution in (k) and (l), similar to the image in (a). Although not obvious in these images except for (i), the "reconnection" of these two axial regimes appears to occur through a connecting helical tube. This process outlined above repeats itself more and more frequently as the flame approaches blow out.

Also evident in these figures are the dynamics of the flame zones near the premixer exit. In (a), no flame is visible in the corner recirculation zone (CRZ) or at the nozzle exit. Moving to (b) and (c), the flame intensities decreases, but combustion is present in the CRZ. These CRZ flames extinguish in (d) and (e), but are sometimes replaced by a sporadically appearing flame that goes almost to the nozzle exit in (d), (f) and several other images. The movement of the flame toward this very high velocity region suggests axial translation of the inner recirculation zone (IRZ), associated with the vortex breakdown bubble.

Measurements of OH chemiluminescence signal collected by an optical fiber directed at the IRZ also show the flame intensity oscillations. During the phase at which the flame intensity is decreasing, it is possible that unburned fuel is entering the combustor, mixing with the burned

hot products and active radicals.   At some point a well-stirred reactor-like region is present which combusts and supplies a 'spark' to reignite the whole flame.

The extinction/reignition process is not periodic, but appears randomly with the average spacing between successive events decreasing as blowout is approached.   Although not shown, measurements of OH chemiluminescence signal shows that the period of this extinction/reignition process varies between 10 – 200 ms for the case in **Figure 41**. Furthermore, each extinction/reignition event does not necessarily follow the identical sequence shown in **Figure 41**.  For example, the flame can just move up and down axially, as in **Figure 41**(a-c).
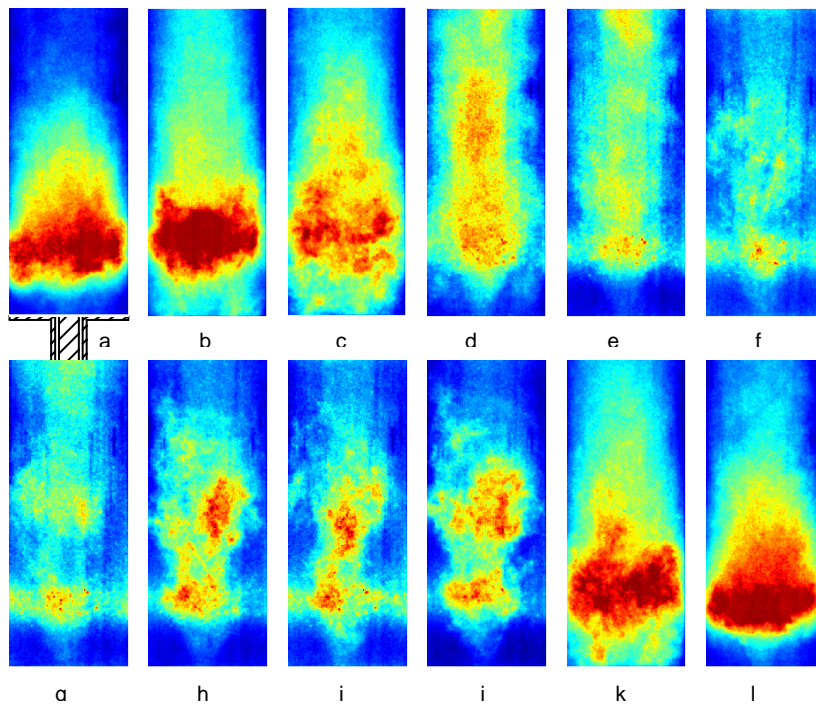


**Figure 41**: **Consecutive images of CH$_4$/Air flame under near blowoff conditions ($\phi$ =0.5; images separation ≈10ms)**
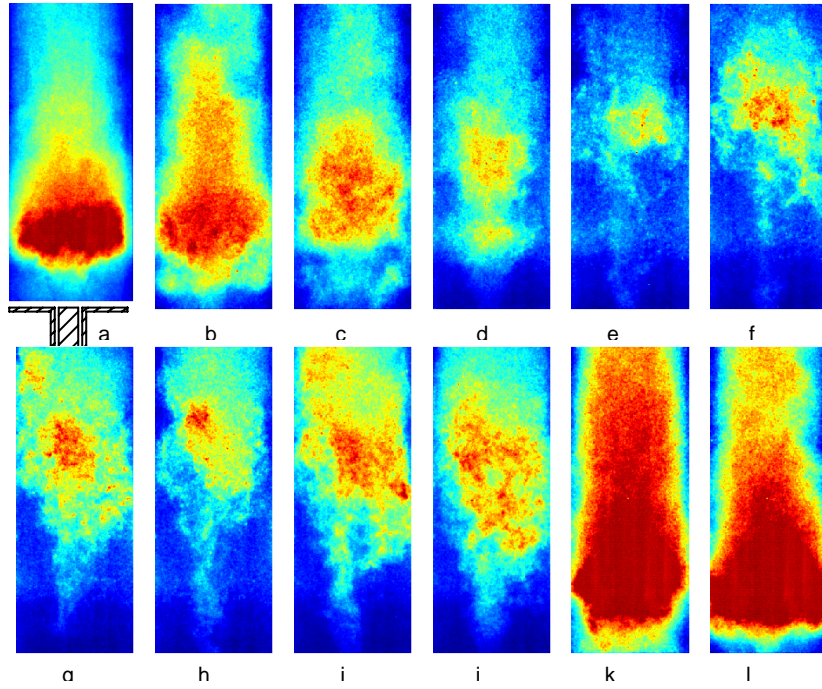
**Figure 42: Consecutive images of 80%CH$_4$ --20% H$_2$ flame under near blowoff conditions (φ =0.42; images separation ≈10ms)**
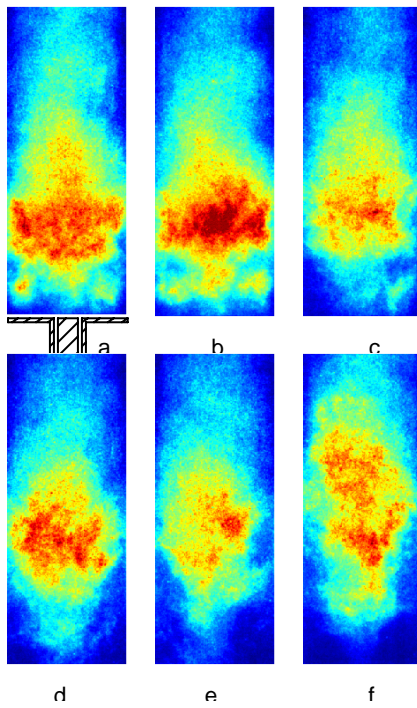


**Figure 43: Consecutive images of 80%CH$_4$ --20% H$_2$ flame under near blowoff conditions (φ =0.42; images separation =2ms)**

Next, consider the effects of $H_2$ addition to the $CH_4$ flame. **Figure 42** shows images for an 80%$CH_4$ -20%$H_2$ flame at $\phi$=0.42. Many of the processes in **Figure 42** and **Figure 41** are very similar but there are some differences. Comparing the lowest intensity levels for $CH_4$ flame (f in **Figure 41**) and 20%$H_2$ addition flame **(**e in **Figure 42**)**,** shows that the lower flame region is of lower intensity (c-d) or in some cases essentially gone (g-i), except for a helical tube that extends downward. Apparently, the strong reignition event in (k) and (l) is precipitated by flame propagation down this tube.

Although we do not fully understand the details, there are some interesting dynamics associated with flame stabilization in the IRZ and CRZ. We hypothesize that the CRZ is normally full of recirculating hot products, with minimal combustion there. As the flame moves downstream, it is anchored by the IRZ (see f-j). However, the CRZ is presumably also now filling with unburned reactants. This region extinguishes and reignites occasionally (see b, c, k), often times with different dynamics than that of the rest of the flame. This reignition can be prompted by flame flashback through the central core region or along the combustor wall by a fluctuation of temperature [40] or just the local turbulent vortex motion [41]. Once reignited, the flame in the CRZ supplies heat and active radicals to the V-flame, helping it reattach to the centerbody or stabilize as a lifted V-flame, see **Figure 43** (a,b). However, by doing so, it "starves" itself of reactants, extinguishes, and then becomes a region of recirculating hot products, such as shown in the sequence of **Figure 43** (a-d). Note also that because the CRZ is located between the combustor wall and the cold dump plate, the heat loss rate is very high, so that the flame in the CRZ quenches easily. Once the CRZ flame is gone, the V-flame loses some of its "pilot" and moves back downstream axially.

Once the mole fraction of $H_2$ is near or higher than 50% by volume, the blowoff phenomenology changes significantly. Like the 20% $H_2$ addition flame, 50% $CH_4$—50% $H_2$ flames still have the extinction/reignition process similar to that in **Figure 42**. Three different sequences of images are shown in **Figure 44, Figure 45, and Figure 46** for a 50%$CH_4$ -50% $H_2$ flame at equivalence ratio of 0.35. Starting with **Figure 44** (a) to (j), the flame intensity weakens gradually and the majority of the radiation intensity moves downstream. A flame is still evident within the helical tube (flame propagation is outward, the center is filled with hot products – evident from the seed density in PIV images), which through either reignition or propagation

downward, propagates back to the nozzle exit. However, in some cases, the flame is not present in this helical tube and is almost completely blown out, before abruptly propagating back upstream, see **Figure 45.**

Flame propagation outward from this columnar tube plays an important role in the re-ignition event, as is particularly evident in **Figure 46,** images (a-g)**.** The flame spreads out and fills the whole combustor, image (e)—(h)**.** However, the fuel/air ratio is apparently too low for the flame to remain stabilized in the entire combustor and the flame reverts back to tornado then columnar shape, image (j)—(l).
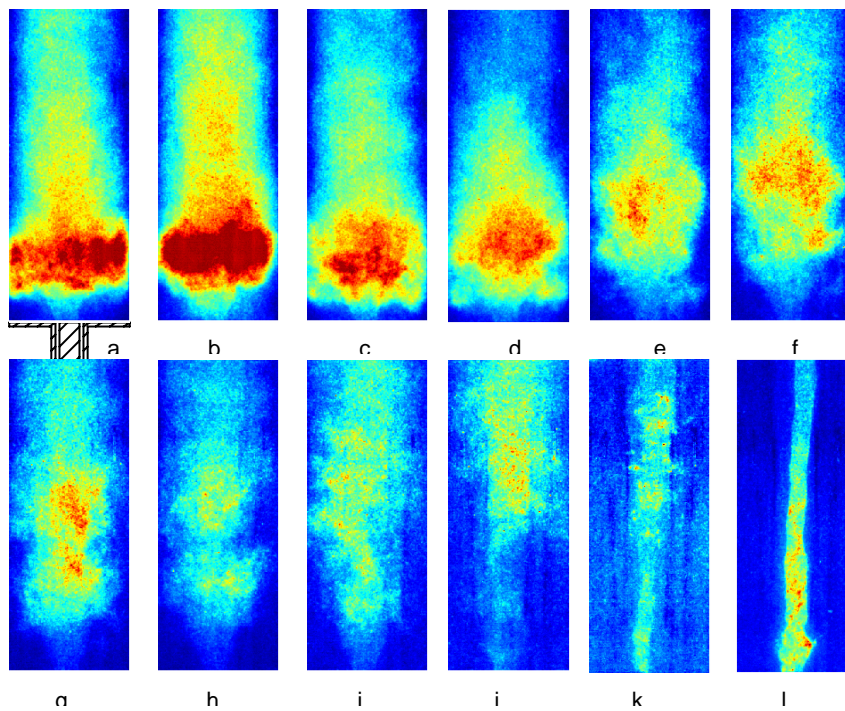


**Figure 44: Consecutive images of 50%CH$_4$ --50% H$_2$ flame under near blowoff conditions (ϕ =0.35; images separation ≈10ms)**
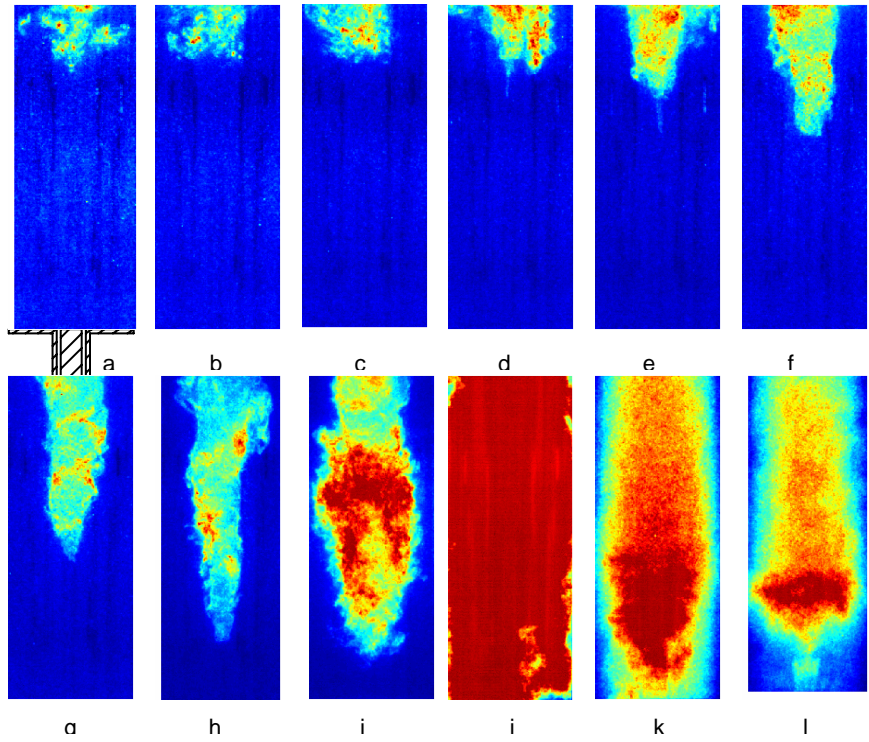
**Figure 45:** Consecutive images of 50%CH$_4$ --50% H$_2$ flame under near blowoff conditions ($\phi$ =0.35; images separation ≈10ms)
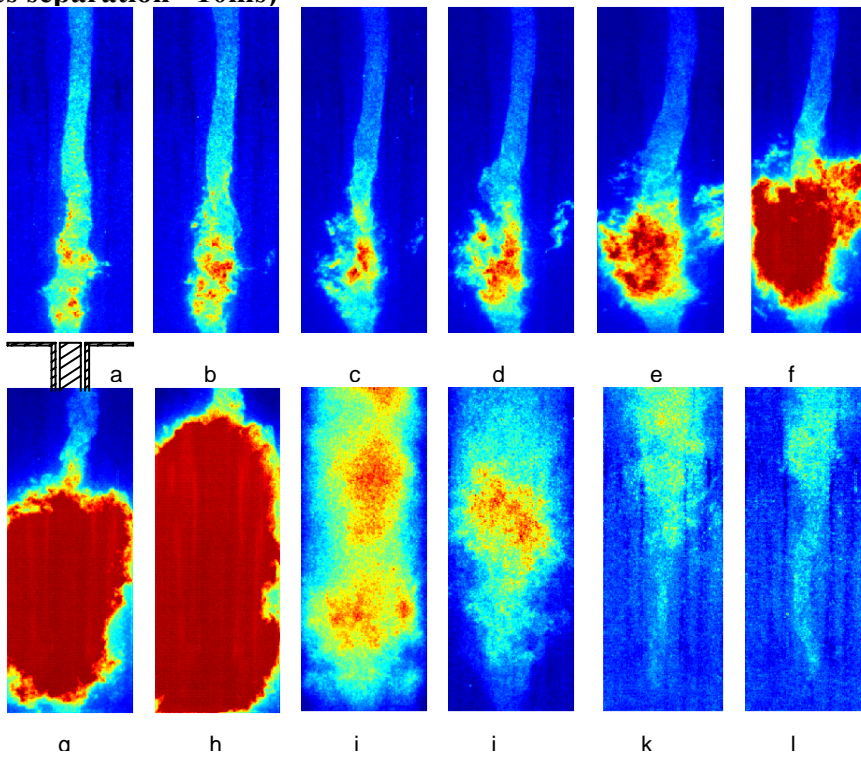
**Figure 46: Consecutive images of 50%CH₄ --50% H₂ flame under near blowoff conditions ($\phi$ =0.35; images separation ≈10ms)**

Further increases in the hydrogen content cause this columnar flame to more and more prominently dominate the flow physics. In fact, at very high $H_2$ levels, the flow prior to blowoff becomes much less unsteady than in the previously shown images, and consists simply of a nearly steady columnar flame (clearly, most of the reactants are exiting the combustor unburned in this situation), see **Figure 47**.
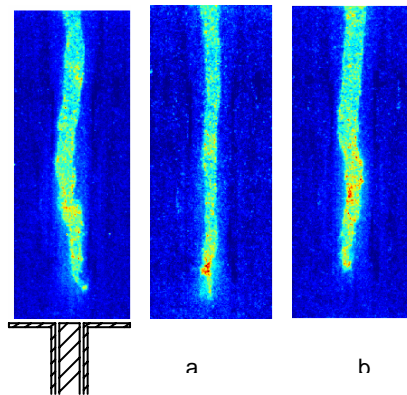


**Figure 47: Consecutive images of 25%CH₄ --75% H₂ flame under near blowoff conditions ($\phi$ =0.31; images separation =10ms)**

**PIV Measurements**

The measured blowoff limits of this system are shown by the black line in Figure 48. The details of test conditions are shown in Table 2.
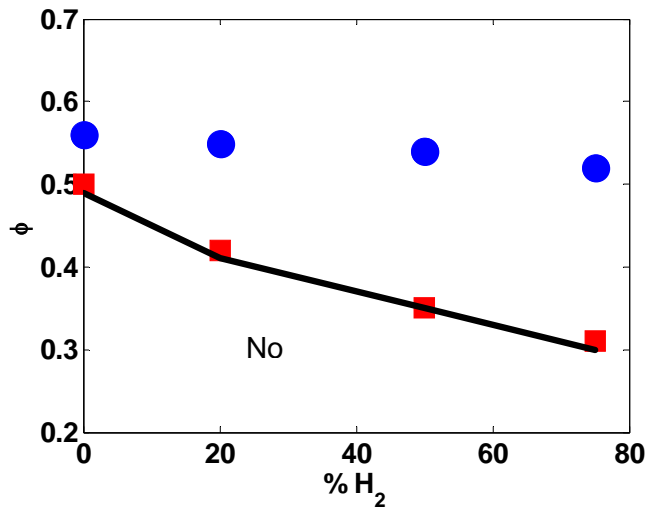


**Figure 48: Dependence of blowoff limits upon percentage of Hygrogen. Constant flame temperature test points shown indicated by blue circles, near blowoff test points indicated by red squares.**

| Fuel Composition (volumetric) | | Constant Temperature Test | | Near Blowoff Tests | |
|---|---|---|---|---|---|
| $H_2$ | $CH_4$ | $\Phi$ | $T_{ad}$ (K) | $\Phi$ | $T_{ad}$ (K) |
| 0 | 100 | 0.56 | 1595 | 0.5 | 1480 |
| 20 | 80 | 0.55 | 1587 | 0.42 | 1329 |
| 50 | 50 | 0.54 | 1594 | 0.35 | 1201 |
| 75 | 25 | 0.52 | 1595 | 0.31 | 1141 |

**Table 2: Test conditions in PIV measurements**

*Averaged Flow Field*

In order to obtain a feel for the basic structure of the swirling flow with or without combustion, time averaged measurements of the cold flow and stable CH$_4$ flame are shown in **Figure 49** (b). Some velocity vectors were removed in areas with significant number of spurious vectors at locations of window reflections. In addition, iso-vorticity lines are also indicated. The 2D vorticity was defined as,

$$\omega = \frac{\partial v}{\partial x} - \frac{\partial u}{\partial y} \qquad (2)$$

where $x$ and $y$ are the radial and axial coordinates, and $u$ and $v$ are the radial and axial velocities, respectively. For clarity, only high magnitude values, $|\omega| > 4000$ s$^{-1}$, are plotted.



(a)                                                              (b)
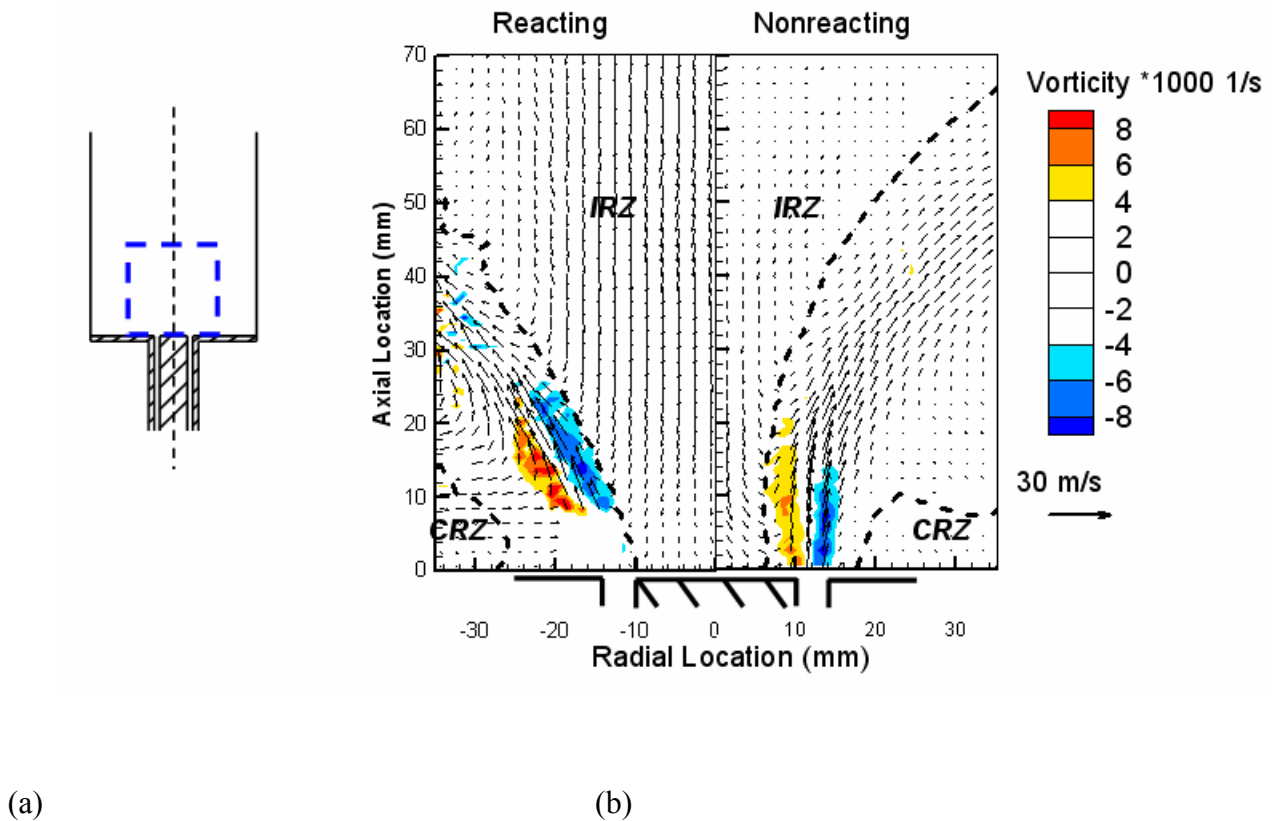
**Figure 49: PIV window arrangement (a) and averaged flow fields (b) of non-reacting flow (right) and reacting flow (stable methane flame, left)**

The bottom boundary is the inlet plane of the combustor, and the centerline is the axis of the combustor. To compare the flow structures with and without combustions, half of each measurement volume is shown, with the nonreacting and reacting on the right and left sides, respectively. Each of the plots is the average of 128 images, sufficient for good convergence [17,43]. The inlet annulus is located between 10 and 14 mm radially.

In both the reacting and non-reacting flow situations, the same basic time averaged flow structure is observed, consisting of a corner recirculation zone (CRZ, due to the rapid expansion), inner recirculation zone (IRZ, due to the vortex breakdown bubble) and an annular jet. The annular jet flow is directed downstream and somewhat outward and separates the IRZ and ORZ. The IRZ and ORZ locations were quantified by the locus of points with zero vertical velocity. Note that the IRZ is merged with the small separation zone downstream of the centerbody [42]. These three flow regimes are separated by two layers of strong, oppositely signed shear, as can be seen from the overlaid vorticity iso-contours.
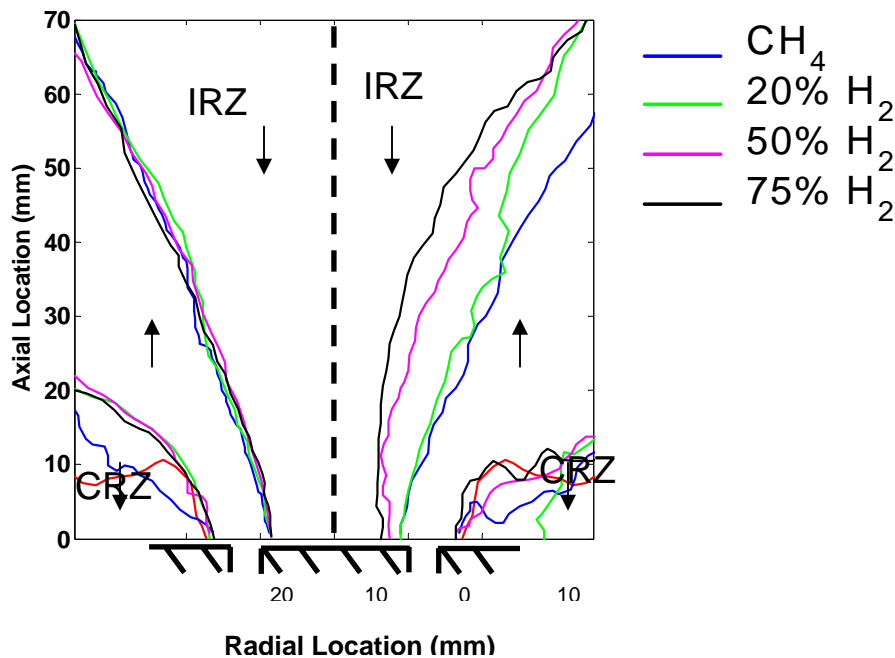


**Figure 50: Contour lines of zero mean axial velocity for flames at the same adiabatic flame temperature (Left half) and near blowoff (Right half).**

Although these three basic flow features are common to the nonreacting and reacting flows, their quantitative characteristics/locations vary significantly. The recirculation zones have much stronger velocity fields in the reacting case, and the IRZ zone is much wider. Therefore, the two shear layers are stronger, as manifested by the larger vorticity magnitudes. In addition, the annular jet region is somewhat narrower in the reacting case. These observations are consistent with others in these types of flows [43].

In order to better understand the relative role of chemical kinetics and fluid mechanics in this system, a set of data were obtained where the relative $H_2/CH_4$ mole fractions were varied, but by adjusting the overall mixture stoichiometry such that the gas expansion ratio across the flame and adiabatic flame temperature (calculated) remained nearly constant at 1590K. These test points are shown in **Figure 48**. Details of the stoichiometries and test conditions are shown in the Table 2. Results illustrating the time averaged location of the IRZ and CRZ boundaries are shown in the left half of **Figure 50.** These results show that all four reacting cases have essentially identical IRZ boundaries, regardless of the fuel $H_2/CH_4$ ratio. This result suggests that kinetic effects do not impact the average flow field structure of constant temperature flames– rather, that it is controlled by the thermal expansion ratio across the flame.

Because the flames with higher hydrogen levels blow out at lower fuel/air ratio's and flame temperatures, the thermal expansion ratio across the flame is different for the near blowoff flames we consider in this report; these test points are illustrated in **Figure 48**. Although the flame shows a strongly dynamic behavior when blowoff is approached, for completeness we plot the corresponding flow boundaries for the near blowoff cases in the right half of **Figure 50.** This figure shows that the size of the IRZ reduces as the percentage of $H_2$ increases, apparently corresponding to the decrease in expansion ratio across the flame. *As such, the fluid mechanic structure of the flow for the near blowoff flames considered in more detail below certainly varies with the fuel composition, not directly due to kinetic effects but due to the lower flame temperature near blowoff.*

(a)  (b)

(c )  (d)
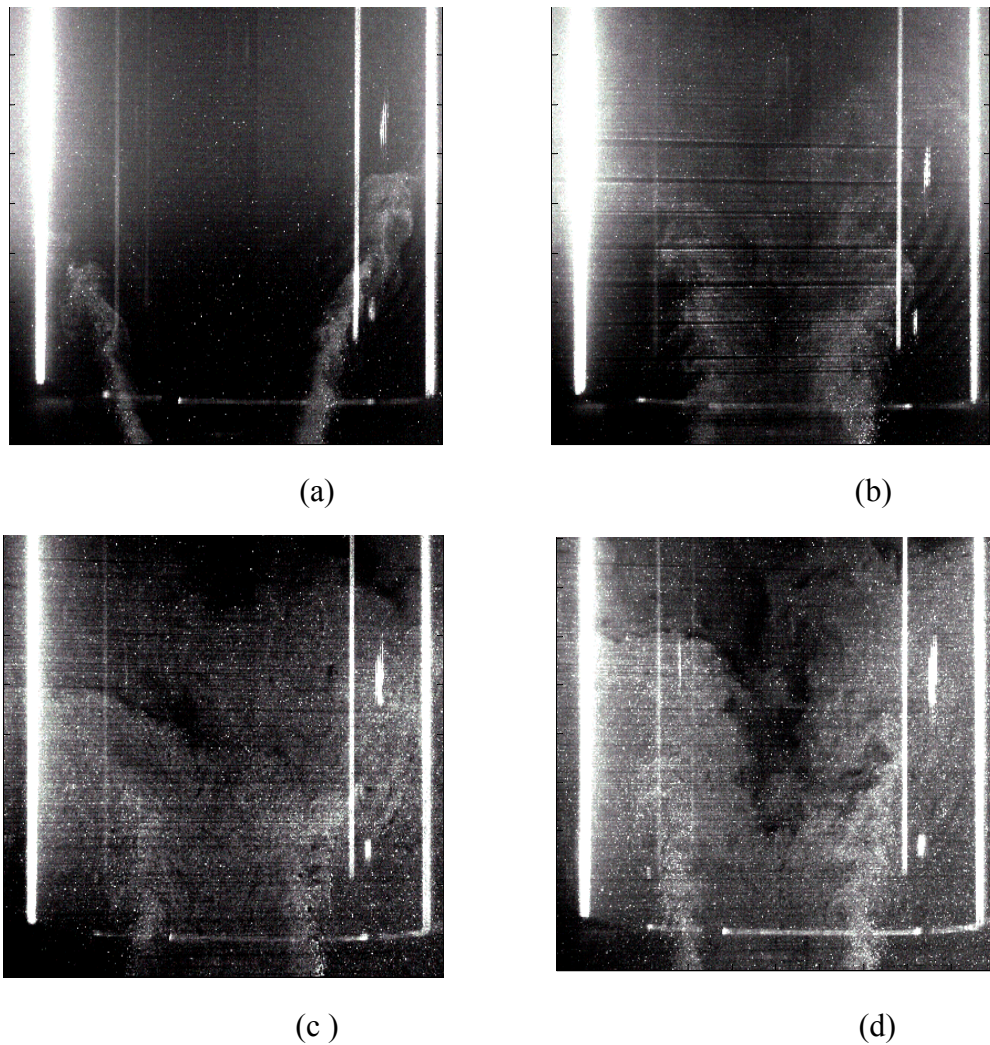
**Figure 51: Typical raw PIV Mie scatting images for CH$_4$ flame near blowoff.**

A group of typical raw Mie scatting images are shown in **Figure 51.** As discussed in our previous section, a flame near blowoff tends to exhibit substantial dynamics, including apparent extinction-ignition behavior. Unfortunately, it is difficult to discern the reaction zone location during these events because of local "holes" in the flame sheet and a highly disorganized field of reactant/product interfaces – in cases where the flame sheet is largely continuous, its location can be easily determined by simultaneous analysis of the seed density and its gradient. The latter situation is the case at points where the flame is stabilized on the centerbody or downstream,

such as shown in **Figure** 51 **(a).** However, the flame bounces between these two states for the majority of the time near blowoff (around 90% of the raw images for the low $H_2$ cases), and it is quite difficult to mark the reaction zone, see **Figure 51 (b,c,d )**. In such a phase, the flame surface has holes which cause the cold reactants to mix with the hot products. In the subsequent discussion, we focus on images where the flame front can be tracked along with the flow field. It should be recognized that this necessarily excludes the majority of images. It does, however, allow us to understand the two flame states that the system is oscillating between, which are separated by rather chaotic periods of disorganized product/reactant interfaces.

**Figure** 52 shows four typical instantaneous velocity fields for a $CH_4$ flame at equivalence ratio of 0.5, which is near blowoff. The solid black line represents the flame front near the nozzle exit, which is determined from the steep gradient in seed density. This approach for discerning the flame position only works well in the near nozzle region, however, and it is more difficult to discern the flame edge farther downstream. As such, although the lines indicating the flame front stop at some downstream/radial location, the flame persists farther beyond it. Many of the basic flow features described above are still discernable from these images. The annular jet extends downstream and radially outward, whose edges are demarcated by the regions of high shear and vorticity. At the center of the combustor, a strong backflow indicates the IRZ, and the CRZ is evident in the two corners. However, a number of fine scale vortex flow features are observed in these images which are averaged out in the images shown above. In particular, the jet and shear layers are distorted greatly by the small vortices (same order of the radius of the centerbody). In two of the images (a) and (d), the flame is attached to the centerbody, similar to prior observations [43]. The flame is stabilized in this high shear region and extends radially outward along the high shear, inner edge of the annular jet. Higher vorticity levels are observed instantaneously than on average; e.g., the instantaneous vorticity in the shear layers is around 16,000 $s^{-1}$, while it is 8,000 $s^{-1}$ in the averaged field, see **Figure 49**.

In two of the images, (b) and (c), the flame is not attached to the centerbody and is situated downstream. It is stabilized in these cases by the recirculating flow in the IRZ. The centerbody wake flow is substantially altered in these two cases, as a much longer wake is evident. In contrast, when the flame is attached to the centerbody, the strong thermal expansion induced flow across the flame renders this wake region nearly unrecognizable. The CRZ region has multiple fine vortices. For example a pair of vortices, which have opposite senses, occupy the

corner region, see the right corner of **Figure** 52 **(c).** The sense of the rotation of the bottom vortex is counter-clockwise, which is opposite with the direction of high speed jet. It shows that the instantaneous fine vortices have different or even opposite properties than the averaged main flow structure. The bottom of the flame is inside the IRZ, and extends radially outward. In both images, however, the flame is clearly located downstream and inside the inner shear layer. This suggests that this image is only a snapshot of a dynamic phenomenon where the whole flame is for a few instances being blown downstream. Unfortunately, the sampling rate of the PIV system is not high enough to capture multiple images of a single one of these events
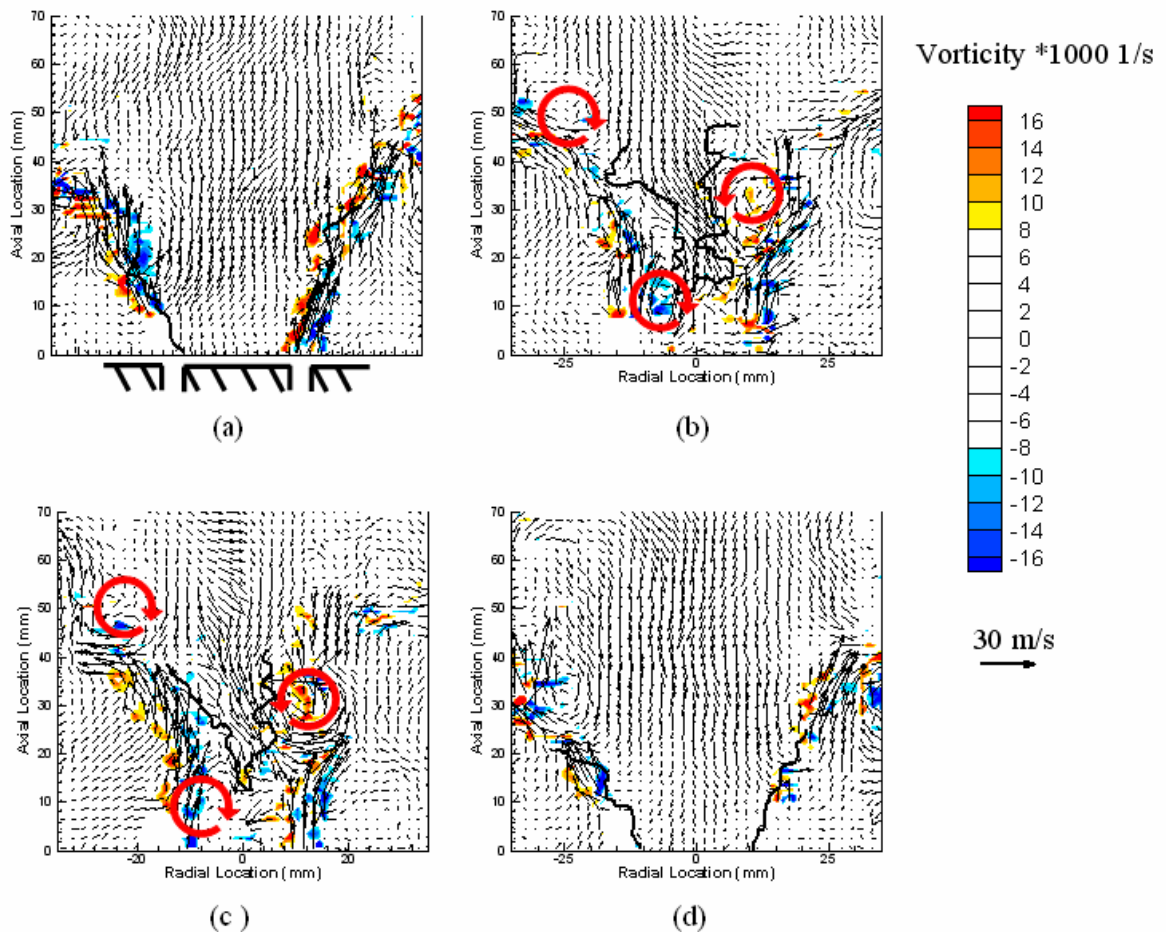


**Figure 52: Instantaneous flow field and flame front for CH$_4$ flame near blowoff.**

Notice also that the flame front is substantially more corrugated in these instances when it is located downstream, due to wrinkling from the fine scale vortices alluded to above. These vortices may be associated with a helical vortex tube that spirals downstream, see red circular

arrows in **Figure** 52 (b, c). Interestingly, these same vortices are not evident in images (a) and (d), where the flame is attached to the centerbody, **Figure** 52 (a, d). This suggests a complete restructuring of the dynamic flow field due to thermal expansion effects and fundamentally different flow features when the flame is and is not attached to the centerbody.

The previous section has consistently showed that near blowoff flames are quite unsteady and oscillate between "extinction" and "re-ignition" phases near blowoff. These images depict one of these unsteady phases, and show that, at least in this case, they are associated with an oscillation between two stabilization points, separated by local-extinction/reignition and product/reactant mixing. Presumably, the local strain rate at the flame attachment point becomes too high and the flame locally extinguishes, causing it to blow downstream. During this process, reactants can penetrate the wake region, causing substantial product-reactant mixing and making the reaction zone region unintelligible. Farther downstream, the two flame branches merge and, after some transient, the flow is again divided into regions of only high and low seed density – making it possible to determine flame location. This flame then moves back upstream. Notice that the velocity vectors in these cases are pointing upstream, showing that the flame is moving upstream. Interestingly, we have almost no images where the post flame velocity field is moving downstream. This shows that during these instances of downstream movement, substantial product-reactant mixing is present and the reaction location is not discernable.

Figure 53 shows the four typical instantaneous velocity fields for a near blowoff flame, consisting of 50%$CH_4$ /50% $H_2$ at an equivalence ratio of 0.35. Note that this corresponds to a lower flame temperature than the pure methane result. A similar flow structure and dynamical sequence of events is observed in **Figure** 53 as in **Figure** 52. The flame is also stabilized in the inner shear layer, when the flame is attached to the centerbody, see **Figure** 53 **(a,d)** and by the recirculating flow when it is lifted off, see **Figure** 53 **(b,c).**
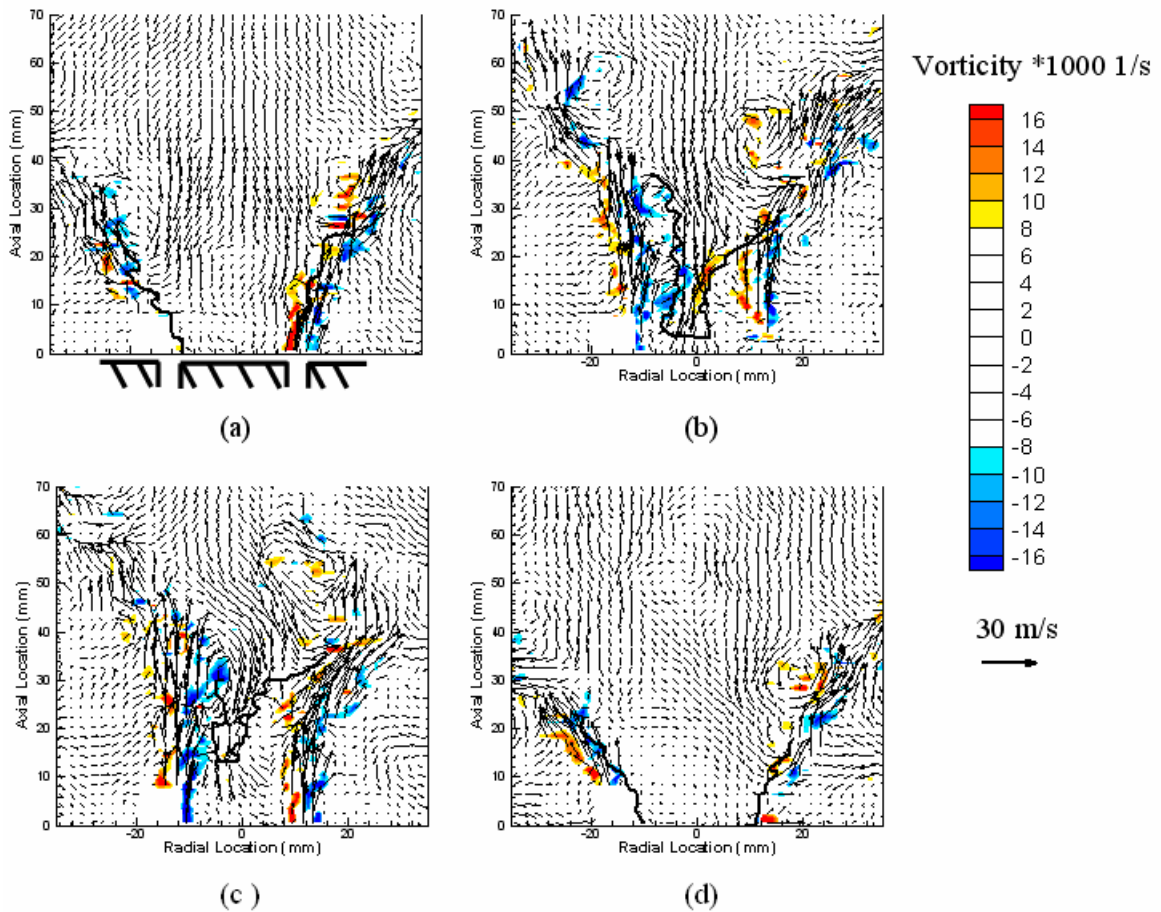
**Figure 53: Instantaneous flow field and flame front for 50%CH₄ /50% H₂ flame near blowoff.**

Higher hydrogen level flames near blowoff exhibit different dynamics because they never are stabilized on the inner centerbody shear layer, but only downstream. Furthermore, the flame exhibits a thin, columnar shape, evident in some cases in the 50%/50% case. Further increases in the hydrogen content cause this columnar flame to more and more prominently dominate the flow physics. In fact, at very high $H_2$ levels, the flow prior to blowoff becomes much less unstable, and consists simply of a nearly steady columnar flame (clearly, most of the reactants are exiting the combustor unburned in this situation). This is associated with a substantially higher percentage of the images having clear seed density interfaces corresponding to the flame – roughly 50%. Although these images closely resemble those shown above in cases where the flame is downstream, this point should be kept in mind as the more typical, larger number of events are not shown. **Figure** 54 shows four typical results for 25%CH₄ /75% H₂ flame at an equivalence ratio of 0.31, which is close to the blowoff limit. A columnar flame is not obvious

in this plot due to only a small part of the flame is plotted; however, it is very obvious from direct visualization. A columnar flame stabilized near the nozzle and extends to the exit of the combustor.
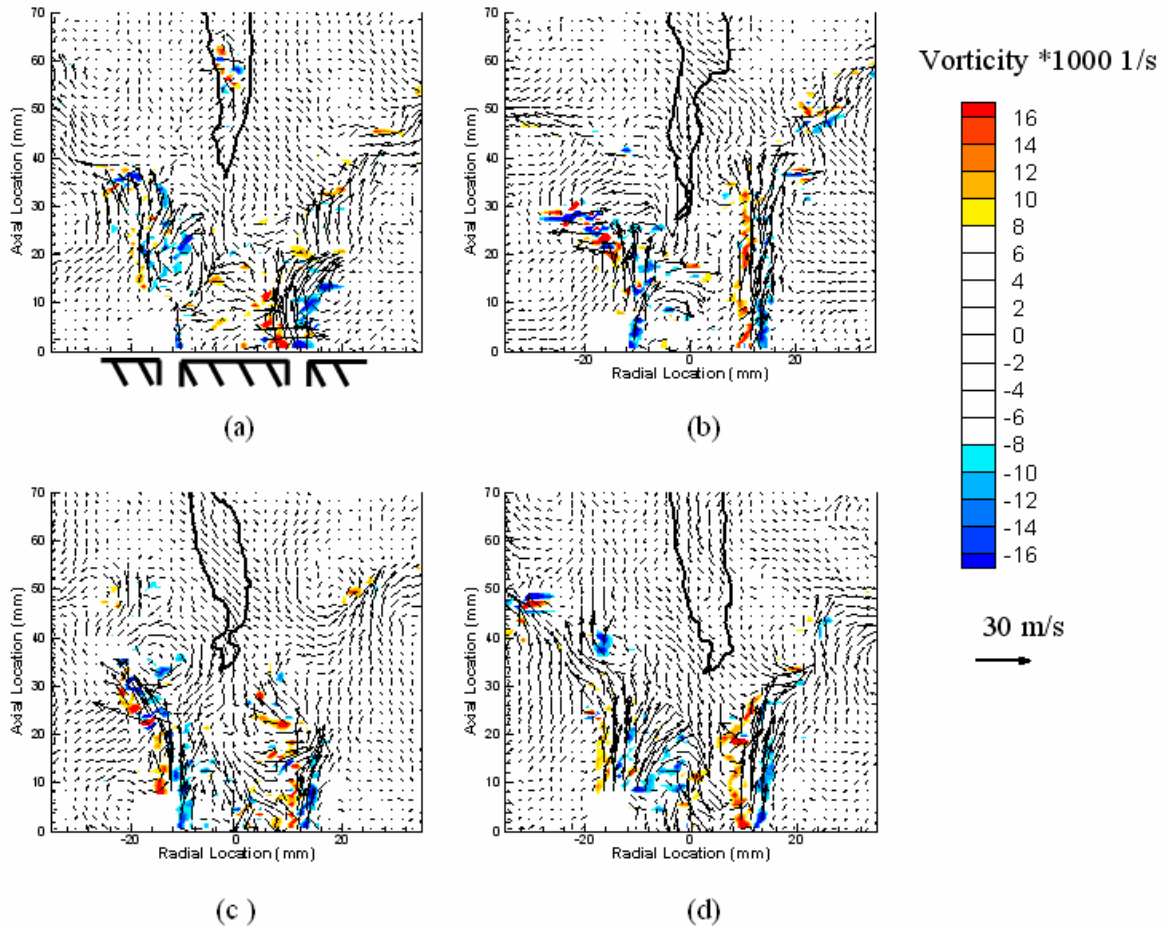


**Figure 54: Instantaneous velocity field and flame front for 25%CH$_4$ /75% H$_2$ flame near blowoff.**

This PIV image shows many of the same basic features as described in the earlier cases. There are some hot products between the bottom of the flame and the centerbody, which are determined by low seed density regions, see red circles in **Figure 55**. Normally, the hot products exist as small, unconnected wrinkled regions. Analysis of the seed density gradient suggests that these interfaces are not flame fronts.

<div align="center">(a)            (b)</div>
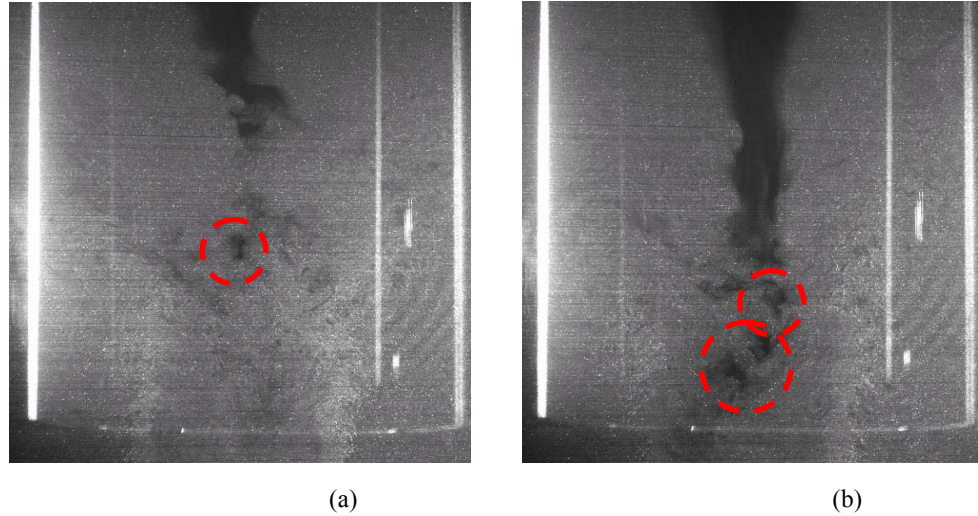
**Figure 55: Raw Mie scatting images in PIV measurements for 25%CH$_4$ /75% H$_2$ flame near blowoff.**

An important question relates to the relative roles of fluid mechanics and chemical kinetics in causing the above described variation in near blowoff phenomenology. Fluid mechanics certainly exert some role as the average gas expansion ratio monotonically decreases as the H$_2$ levels increase, due to the lower flame temperatures these mixtures can sustain, see **Figure 50**. This variation in gas expansion ratio and flow velocity must cause some variations in the fluid mechanics of the flow.

Kinetics, particularly strain sensitivities, certainly exerts a role on the dynamic oscillation between the attached and unattached flames shown for the lower hydrogen level flames. These flames were never observed to persist downstream in the steady state, as was observed with higher hydrogen flames. It seems likely that the strain that the flame is subjected to is substantially lower downstream, so this is a puzzling result. In contrast, high H$_2$ flames under very near blowoff conditions are never observed to attach to the centerbody, suggesting that the local strain rate exceeds the extinction value. However, the flame can exist downstream. For example, many PIV images clearly show the flame interface right at the boundaries of high vorticity regions (this could also reflect the reduction in vorticity across the flame, however). Perhaps one of the reasons for the lack of a stable downstream configuration with low H$_2$ flames, in contrast to high H$_2$ flames, is the different flow field in the two situations because of the differing flame dilatation ratios.

It is well known that $H_2$ addition substantially increases the extinction strain rate of $CH_4$ flames. The situation is more complex when comparing near blowoff flames because the flame temperature and stoichiometry monotonically decreases with increasing $H_2$ levels – possibly the extinction strain rate of the high $H_2$ flames near blowoff is lower than the lower $H_2$ flames.

# 8.    Concluding Remarks

Both expected and unexpected results were obtained from this study.  First, the finding that blowoff limits were broadened with $H_2$ addition was expected and very consistent with other experience.  However, the ability of the simple parameter, percentage of $H_2$, to correlate data over such a broad range of conditions and fuel compositions was surprising.    Furthermore, the way in which the dynamics of the blowoff process changed in such a significant qualitative manner with $H_2$ levels was unexpected, but further demonstrated the rich character of the problem, involving complex interactions between kinetics and fluid mechanics.

Future studies are needed to further elucidate the subtle interactions between flame dilatation ratio and chemical kinetics on these blowoff dynamics.  In addition, this study has highlighted the poor understanding of the dynamics of swirling flow dynamics, even for well stabilized flames.  Continued study of swirling flow dynamics should be a key focus of the community, as these dynamics play such a prominent role in the observed flames.

# 9. REFERENCES

[1] Langston, Lee, "Gas Turbine Industry Overview", in 2001 IGTI Technology Report and Product Directory, ASME 2001.

[2] Correa, S.M., Power Generation and AeroPropulsion Gas Turbines: From Combustion Science to Combustion Technology, *Twenty Seventh Symposium (International) on Combustion*, The Combustion Institute, Pittsburgh, PA, 1998.

[3] Klimstra, Jacob, Interchangeability of Gaseous Fuels – The Importance of the Wobbe Index, *SAE paper # 861578*, 1986.

[4] King, Steve, The Impact of Natural Gas Composition on Fuel Metering and Engine Operating Characteristics, *SAE paper # 920593*, 1992.

[5] Durbin, M., Ballal, D., "Studies of Lean Blowout in a Step Swirl Combustor", *J. Engr. Gas Turbines and Power*, Vol. 118, 1996.

[6] Barlow, R.S., Fiechtner, G.J., Carter, C.D., Chen, J.Y., "Experiments on the Scalar Structure of Turbulent $CO/H_2/N2$ Jet Flames", *Comb. Flame*, Vol. 120, 2000.

[7] Correa, S.M., Gulati, A. "Non-premixed Turbulent CO/H2 flames at local extinction conditions", *Proc. Comb. Inst.* Vol. 22, 1988, pp. 599-606.

[8] Drake, M.C., "Stretched Laminar Flamelet Analysis of Turbulent H2 and $CO/H_2/N_2$ Diffusion Flames", *Proc. Comb. Inst.*, Vol. 21, 1986, pp. 1579-1589.

[9] Correa, S.M., Gulati, A., Pope, S.B., "Assessment of a Partial Equilibrium/Monte Carlo Model for Turbulent Syngas Flames", *Comb. Flame*, Vol. 72, 1988, pp. 159-173.

[10] Masri, A. R., Dibble, R. W., "Spontaneous Raman Measurements in Turbulent CO/H2/N2 Flames Near Extinction", *Proc. Comb. Inst.* Vol. 22, 1988, pp. 607-618.

[11] Glassman, I., *Combustion*, Academic Press: New York, 1996.

[12] Sankaran, Ramanan, Im, Hong G, "Dynamic Flammability Limits of Methane/Air Premixed Flames with Mixture Composition Fluctuations", *Proc. Comb. Inst.,* Vol. 29, 2002, ,pp. 77-84

[13] Jackson, Gregory S., Sai, Roxanne, Plaia, Josephi M., Boggs, Christopher M., Kiger, Kenneth T., , "Influence of $H_2$ on the Response of Lean Premixed $CH_4$ Flames to High Strained Flows", *Comb. Flame,*, 132, 2003, pp. 503-511

[14] Vagelopoulos, C.M., Egolfopoulos, F.N., "Laminar Flame Speeds and Extinction Strains Rates of Mixtures of Carbon Monoxide with Hydrogen, Methane, and Air", *Proc. Comb. Inst.,* 1994, pp 1317

[15] Maloney, D., "The Simulation Validation Project at NETL", DOE Report, 2002.

[16] Schefer, R. W., "Hydrogen Enrichment for Improved Lean Flame Stability", *International Journal of Hydrogen Energy,* 28, 2003, pp. 1131-1141.

[17] Wicksall, D., Agrawal, A., "Effects of Fuel Composition on Flammability Limit of a Lean, Premixed Combustor", *ASME Paper #2001-GT-0007*

[18]Zukoski, E.E., "Afterburners", in Aerothermodynamics of Gas Turbine and Rocket Propulsion, G. Oates, Ed., 1997.

[19]Spaulding, D., "Some Fundamentals of Combustion", Ch. 5, Butterworth Press: London, 1955

[20]Longwell, J., Frost, E., Weiss, M., "Flame Stability in Bluff-Body Recirculation Zones", *Ind. Eng. Chem*., Vol. 45 (8), pp. 1629-1633.

[21]Plee, S.L, Mellor, A.M., "Characteristic Time Correlation for Lean Blowoff of Bluff Body Stabilized Flames", *Comb. Flame,*, 35, 1979, pp. 61-80.

[22]Radhakrishnan, K., Heywood, J., Tabaczynski, R., "Premixed Turbulent Flame Blowoff Velocity Correlation Based on Coherent Structures in Turbulent Flows", *Comb. Flame,*, 42, 1981, pp. 19-33.

[23] A.A. Putnam, R.A. Jensen, "Appplication of Dimensionless Numbers to Flash-back and Other Combustion Phenomena" , *Proc. Comb. Inst*., 3rd, 1949, ,pp 89-98

[24] S. Hoffmann, P. Habisreuther, B. Lenze, "Development and Assessment of Correlations for Predicting Stability Limits of Swirling Flames", *Chemical Engineering and Processing*, 33 (1994), pp 393-400

[25]Kido, Hiroyuki, Nakahara, Masaya, Nakashima, Kenshiro, Hashimoto, Jun, "Influence of local flame displacement velocity on turbulent burning velocity**,** *Proc. Comb. Inst*., Vol. 29, 2002, pp. 1855-1861

[26]Paul Clavin, "Dynamic Behavior of Premixed Flame Fronts in Laminar and Turbulent Flows", *Prog. Energy Comb. Sci.,*Vol.11,1985,pp.1-59

[27]Chen, Jacqueline H., Im, Hong G., "Stretch Effects on the Burning Velocity of Turbulent Premixed Hydrogen/Air Flames**,** *Proc. Comb. Inst*., Vol. 28, 2000, ,pp 211-218

[28]Lieuwen, T., Torres, H., Johnson, C., Daniel, B.R., Zinn, B.T., "A Mechanism for Combustion Instabilities in Lean Premixed Gas Turbine Combustors", *Journal of Engineering for Gas Turbines and Power*, 123(1), 2001, pp. 182-190

[29]J. Natarajan, S. Nandula, T. Lieuwen and J. Seitzman, "Laminar Flame Speeds of Synthetic Gas Fuel Mixtures", *ASME Paper # GT2005-68917.*

[30] Kee RJ, Warnatz J, Miller Ja. "A FORTRAN Computer Code Package for the Evaluation of Gas-Phase Viscosities, Conductivities, and Diffusion Coefficients." *Technical Report SAND89-8009*, Sandia National laboratories, 1983.

[31] G.Joulin, T.Mitani, " Linear Stability Analysis of Two-Reactant Flame", *Comb. Flame*,40,1981,pp.235-246

[32] Masaya Nakahara, Hiroyuki Kido, " A Study of the Premixed Turbulent Combustion Mechanism Taking the Preferential Diffusion Effect into Consideration", *Memoirs of the Faculty of Engineering*,  Kyushu Univ., 58, 1998

[33]  Kido, Hiroyuki, Nakahara, Masaya, "A Model of Turbulent Burning Velocity Taking the Preferential Diffusion Effect into Consideration," *JSME International Journal*, Vol. 41, No.3, 1998, pp. 666-673

[34] Nair, S., Lieuwen, T., "Acoustic Detection of Blowout in Premixed Flames" ", *J. Propulsion and Power*, Vol 21, No. 1, P32-39

[35] Nair, S., Rajaram, R., Meyers, A., Lieuwen, T., Tozzi, L., Beson, K., " Acoustic and Ion Sensing of Lean Blowout in an Aircraft Combustor Simulator", *43rd AIAA Meeting Papers*, 2005, p 3627-3634

[36] Muruganandam, T., Kim,B., Olsen, R., Patel, M., Romig, B., and Seitzman, J., "Chemiluminescence based sensors for Turbine Engines", *AIAA-2003-4490*, 2003

[37] Muruganandam, T.M., Nair, S., Scarborough, D., Neumeier, Y., Jagoda, J, Lieuwen, T., Seitzman, J., Zinn, B., " Active Control of Lean blowout for Turbine Engine Combustors", *J. Propulsion and Power*, Vol. 21, No. 5, pp. 807-814.

[38] Lilley, D. G., " Swirl Flows in Combustion: a Review", *AIAA J.* vol 15, No. 8, 1977

[39] Raffel, M., Willert, C. and Kompenhans, J. "Particle image Velocimetry: A Practical Guide", Springer, 1998 (3rd edition).

[40] Yang, V., Huang, Y., "Bifurcation of Flame Structure in a Lean-Premixed Swirl-Stabilized Combustor: Transition from Stable to Unstable Flame", *Comb. Flame*, 136, 2004, pp. 383-389

[41] Bradley, D., Gaskell, P. H., Gu, X. J., Lawes, M., Scott, M. J., "Premixed Turbulent Flame Instability and NO Formation in a Lean-Burn Swirl Burner", *Comb. Flame*, 115, 1998, pp. 515-538

[42] Huang, Ying, Yang, Vigor, " Swirling Flow Structures and Flame Characteristics in a Lean –Premixed Combustor", AIAA-2004-0978

[43] Ji, Jun, Gore P. Jay, " Flow Structure in lean Premixed Swirling Combustion", *Proc. Comb. Inst*., Vol. 29, 2002, pp. 861-867